Studies of Dihadron Electroproduction in DIS with Longitudinally Polarized Hydrogen and Deuterium Targets

(A CLAS12 Run Group C Addition Proposal)

H. Avakian[a],[1] A. Courtoy,[2] C. Dilks[a,b],[3] K. Griffioen,[4]
T. Hayward,[4] M. Mirazita,[5] O. Soto[a],[5] and A. Vossen[3, 1]

[1] *Thomas Jefferson National Accelerator Facility, Newport News, Virginia 23606*
[2] *Instituto de Física, Universidad Nacional Autónoma de México, 01000 Ciudad de México, Mexico*
[3] *Duke University, Durham, North Carolina 27708*
[4] *College of William and Mary, Williamsburg, Virginia 23187*
[5] *INFN, Laboratori Nazionali di Frascati, 00044 Frascati, Italy*

We propose a comprehensive program to measure dihadron correlations produced in SIDIS to investigate novel aspects of non-perturbative QCD in proton structure and hadronization. Compared to the well-explored single-hadrons observables, dihadron production has an additional degree of freedom which allows for targeted access to quark-gluon correlations in the proton, transverse-momentum dependent parton distributions (TMDs), and previously unexplored spin-orbit correlations in hadronization via the framework of dihadron fragmentation functions (DiFFs). The measurements are proposed to be a part of Run Group C approved experiments, using the CLAS12 detector with an 11 GeV highly-polarized electron beam scattering off a longitudinally polarized target, effectively composed of either hydrogen or deuterium in solid ammonia (NH_3 or ND_3). The CLAS12 detector provides a unique opportunity for this physics program due to its large acceptance, which allows for the simultaneous detection of the scattered electron and dihadron. Target spin asymmetries in dihadrons, as well as double spin asymmetries, are sensitive to spin-orbit correlations in hadronization, as well as TMDs and collinear twist-3 parton distributions; these measurements combined with recent beam spin asymmetries measurements at CLAS12 allow for a cleaner interpretation of their constraints on distribution and fragmentation functions. A comparison of these asymmetries from the hydrogen target to those from the deuterium target is sensitive to the flavor dependence of these distributions. Moreover, the detection of target fragments will allow for the extension of the program into the target fragmentation region (TFR). An analysis of correlations between a hadron produced in the TFR with a hadron in the current fragmentation region (CFR) is sensitive to the fracture functions, which encode the probability of finding a parton in a nucleon fragmenting into a particular hadron. A wide range of fracture functions is accessible in target spin, beam spin, and double spin asymmetries of this class of dihadrons. The large acceptance at CLAS12 provides a unique opportunity for several dihadron correlation measurements, and a polarized target extends the program, broadening our overall understanding of the nucleon and the dynamics of its constituents.

---

[a] Co-spokesperson
[b] Contact: dilks@jlab.org

Contents

I. Introduction

In recent years, measurements of azimuthal moments of polarized hadronic cross sections in hard processes have emerged as a powerful tool to probe the nucleon structure. Many experiments worldwide are currently trying to pin down various effects related to the nucleon structure through semi-inclusive deep-inelastic scattering. In fact, the partonic structure of the nucleon and other fundamental aspects of QCD as well as the hadronization processes are at the core of the physics program that motivated the 12 GeV upgrade as well as the future EIC. Azimuthal distributions of final state particles in semi-inclusive deep inelastic scattering, in particular, are sensitive to the orbital motion of quarks and play an important role in the study of transverse momentum distributions (TMDs) of quarks in the nucleon and spin orbit correlations in hadronization. For an overview see Refs. [1, 2].

The primary focus of the measurements in this proposal aims at extracting twist-3 distribution functions $e(x)$ and $h_L(x)$ from longitudinal spin asymmetries; the motivation and procedure are outlined in section II. The functions $e(x)$ and $h_L(x)$, together with the better known twist-2 functions $f_1(x), g_1(x)$ and $h_1(x)$ as well as the twist-3 function $g_T(x)$, completely describe the nucleon structure in a collinear picture up to twist-3. Experimental evidence suggests that they are of sizable magnitude and observables are of similar size as for leading twist quantities at JLab kinematics [3, 4]. They have strong connections to TMDs but contain additional information about non-perturbative QCD dynamics inside the nucleon.

Longitudinal spin asymmetries are also sensitive to dihadron fragmentation functions, in particular to the helicity-dependent fragmentation function $G_1^\perp$, discussed in section III. Measuring target spin asymmetries, in addition to beam spin asymmetries, will help constrain $G_1^\perp$. Furthermore, spin asymmetries are sensitive to the partial wave expansion of the dihadron fragmentation functions, which can shed light on correlations between fragmenting quark polarization and the final state angular momentum of the dihadron.

Another aim of this proposal is to explore correlations between the current and target fragmentation regions to access fracture functions. Recent theoretical work [5] highlighted that the knowledge of these functions is essential to understand particle production over a large part of the kinematical phase space covered by the JLab DIS experiments. The related measurements are discussed further in section IV.

Section V follows through with a description of the experiment and the analysis technique. Section VI starts by highlighting recent measurements relevant to this proposal, and ends with statistical projections of the proposed measurements. Finally, the summary is given in section VII.

We note that this proposal is in large part an update of [6], a PAC38 proposal. This proposal was deferred in favor of higher priority measurements for the first 5 years of 12 GeV operations, but now it is time to revisit the possibility of the proposed measurements. We propose that these measurements take place during Run Group C, in parallel with approved experiments, which include [7–10].

N/q	U	L	T
U	$f^{\perp}$	$g^{\perp}$	h ,e
L	$f_L^{\perp}$	$g_L^{\perp}$	h_L ,e_L
T	f_T , $f_T^{\perp}$	g_T , $g_T^{\perp}$	h_T ,e_T ,$h_T^{\perp}$, $e_T^{\perp}$

TABLE I. Twist-3 transverse momentum dependent distribution functions. The U,L,T correspond to unpolarized, longitudinally polarized and transversely polarized nucleons (rows) and quarks (columns)

II. Collinear dihadron production in the current fragmentation region at twist-3

A. Introduction

Recent theoretical progress on twist-3 TMDs, clarifying the connection to TMDs as well as elucidating their connection to quark-gluon correlations [11], led to renewed interests in these quantities. At twist-3, and before integration over transverse momentum, there are 16 distribution functions; they are shown in table I for different combinations of target (rows) and quark (columns) polarizations. Only three functions survive integration over transverse momentum (collinear functions): e, h_L and g_T. Together with the twist-2 PDFs (f_1, g_1, h_1), they give a detailed picture of the nucleon in longitudinal momentum space. The main goal of the present proposal is to access the functions e and h_L.

Higher twist functions are of interest for several reasons. Most importantly they offer insights into the physics of the largely unexplored quark-gluon correlations which provide direct and unique insights into the dynamics inside hadrons, see, e.g., [12]. They describe multiparton distributions corresponding to the interference of higher Fock components in the hadron wave functions, and as such have no probabilistic partonic interpretations, yet they offer fascinating doorways to studying the structure of the nucleon. The x^2-moment[1] of the twist-3 function $e(x)$ describes the average transverse color force acting on a transversely polarized quark, in an unpolarized nucleon [13]. The x^2 moment of $h_L(x)$ vanishes, but the higher-order x^3 moment describes the average longitudinal gradient of the transverse force that acts on a transversely polarized quark; the sign of this gradient will help to study correlations between the nucleon spin and its color magnetic field [14].

Higher twist contributions are also indispensable to correctly extract twist-2 parts from data. Although suppressed with respect to twist-2 observables by $1/Q$, twist-3 observables are not small in the kinematics of fixed target experiments. This is illustrated by the fact that the single-hadron twist-3 asymmetry $A_{UL}^{\sin\phi}$ is a large and cleanly seen effect, while the twist-2 asymmetry $A_{UL}^{\sin 2\phi}$ is small and compatible with zero in the kinematics of HERMES, JLab, and COMPASS [15–19]. The theoretical description of twist-3 observables is challenging in single-hadron SIDIS. Although lots of effort was devoted to their study [20–35], these observables are still not understood. Partially, this has to do with the problem of formulating a TMD-factorization at twist-3 level [36, 37].

An important process which can provide complementary information on twist-3 TMDs is the dihadron production in SIDIS described by interference functions [38–44]. In fact, the measurement of single-spin asymmetries with a longitudinally polarized target or beam is sensitive in particular to the twist-3 chiral-odd distribution functions e and h_L, in combination with the chiral-odd interference fragmentation function $H_1^{\sphericalangle}$ [42]; the twist-3 distribution functions are collinear and survive integration over the quark transverse momentum. Dihadron production becomes a unique tool to study the higher twist effects appearing as $\sin\phi$ modulations in target or beam spin dependent azimuthal moments of the SIDIS cross section. The interference fragmentation function $H_1^{\sphericalangle}$ has been used to obtain information on the transversity parton distribution function [45].

One of the main sources of systematic uncertainties is the contribution from target fragmentation, which is of its own interest and will be also studied in the proposed measurement. It was shown that the leading order azimuthal asymmetries in the case where one of the hadrons is produced in the target fragmentation region provide access to polarized TMD Fracture Functions, which are conditional probabilities to produce

---

[1] in particular, the moment of the pure twist-3 part of the distribution

a hadron h in TFR when hard scattering occurs on a quark q from the target nucleon N [46, 47]. For these processes for longitudinally polarized lepton scattering, the cross section depends on initial quark longitudinal polarization even if one does not measure the final quark polarization already in leading order.

The JLab 12-GeV upgrade will provide the unique combination of wide kinematic coverage, high beam intensity (luminosity), high energy, high polarization, and advanced detection capabilities necessary to study the transverse momentum and spin correlations in dihadron production in double-polarized semi-inclusive processes both in the target and current fragmentation regions.

B. Observables

We consider the process

$$\ell(l) + N(P) \to \ell(l') + h_1(P_1) + h_2(P_2) + X, \tag{1}$$

where h_1 and h_2 denote the produced hadrons, ℓ the beam lepton and N the nucleon target. The four-momenta are given in parentheses.

In the one-photon exchange approximation and neglecting the lepton mass, the cross section for two-particle inclusive DIS, integrated over the transverse momentum of the produced pair, can be written in the following way [48]:

$$\begin{aligned}
\frac{d\sigma}{dx\,dy\,d\psi\,dz_h\,d\phi_{R_\perp}\,dM_h\,d\cos\theta} &= \frac{\alpha^2}{xy\,Q^2}\left(1+\frac{\gamma^2}{2x}\right) \\
\times \Bigg\{ & A(x,y)\,F_{UU,T} + B(x,y)\,F_{UU,L} + \frac{1}{2}\,V(x,y)\,\cos\phi_{R_\perp}\,F_{UU}^{\cos\phi_{R_\perp}} + B(x,y)\,\cos(2\phi_{R_\perp})\,F_{UU}^{\cos 2\phi_{R_\perp}} \\
& + \lambda_e\,\frac{1}{2}\,W(x,y)\,\sin\phi_{R_\perp}\,F_{LU}^{\sin\phi_{R_\perp}} \\
& + S_L\left[\frac{1}{2}\,V(x,y)\,\sin\phi_{R_\perp}\,F_{UL}^{\sin\phi_{R_\perp}} + B(x,y)\,\sin(2\phi_{R_\perp})\,F_{UL}^{\sin 2\phi_{R_\perp}}\right] \\
& + S_L\lambda_e\left[C(x,y)\,2\,F_{LL} + \frac{1}{2}\,V(x,y)\,\cos\phi_{R_\perp}\,F_{LL}^{\cos\phi_{R_\perp}}\right] \\
& + |\boldsymbol{S}_\perp|\Bigg[\sin(\phi_{R_\perp}-\phi_S)\left(A(x,y)\,F_{UT,T}^{\sin\left(\phi_{R_\perp}-\phi_S\right)} + B(x,y)\,F_{UT,L}^{\sin\left(\phi_{R_\perp}-\phi_S\right)}\right) \\
& \quad + B(x,y)\,\sin(\phi_{R_\perp}+\phi_S)\,F_{UT}^{\sin\left(\phi_{R_\perp}+\phi_S\right)} + B(x,y)\,\sin(3\phi_{R_\perp}-\phi_S)\,F_{UT}^{\sin\left(3\phi_{R_\perp}-\phi_S\right)} \\
& \quad + \frac{1}{2}\,V(x,y)\,\sin\phi_S\,F_{UT}^{\sin\phi_S} + \frac{1}{2}\,V(x,y)\,\sin(2\phi_{R_\perp}-\phi_S)\,F_{UT}^{\sin\left(2\phi_{R_\perp}-\phi_S\right)}\Bigg] \\
& + |\boldsymbol{S}_\perp|\lambda_e\Bigg[C(x,y)\,\cos(\phi_{R_\perp}-\phi_S)\,2\,F_{LT}^{\cos(\phi_{R_\perp}-\phi_S)} + \frac{1}{2}\,V(x,y)\,\cos\phi_S\,F_{LT}^{\cos\phi_S} \\
& \quad + \frac{1}{2}\,V(x,y)\,\cos(2\phi_{R_\perp}-\phi_S)\,F_{LT}^{\cos(2\phi_{R_\perp}-\phi_S)}\Bigg]\Bigg\},
\end{aligned} \tag{2}$$

where α is the fine structure constant, λ_e is the beam polarization, $\boldsymbol{S}$ is the target polarization, with longitudinal component S_L and transverse component $|\boldsymbol{S}_\perp|$. The functions A, B, C, V, W are kinematic depolarization factors (see Appendix A), dependent on the the ratio ε of longitudinal and transverse photon flux [49]:

$$\varepsilon = \frac{1-y-\frac{1}{4}\gamma^2y^2}{1-y+\frac{1}{2}y^2+\frac{1}{4}\gamma^2y^2}. \tag{3}$$

Following the Trento conventions [50] all relevant angles are defined on figure 1 [41].[2] The final hadrons' invariant mass M_h is assumed to be much smaller than the hard scale $Q^2 = -q^2 \geq 0$ $(q = l - l')$ of the SIDIS process, defined by kinematic variables $x = Q^2/2\,P\cdot q$, $y = P\cdot q/P\cdot l$, $z = P\cdot P_h/P\cdot q$ and $\gamma = 2Mx/Q$. With P_1 and P_2 denoting the hadron momenta, $P_h = P_1 + P_2$ and $R = (P_1 - P_2)/2$ denote the pair total momentum and relative momentum, respectively. Finally, this cross section is integrated over dihadron transverse momentum $P_{h\perp}$, and the angle ϕ_h, defined as the angle between the lepton scattering plane and the plane spanned by P_h and q.

The structure functions on the r.h.s. depend on x, Q^2, z, $\cos\theta$, and M_h^2. The angle θ is defined in the center-of-mass of the two hadrons, where the hadron emission occurs back-to-back; it is defined as the angle between the direction of emission and the direction of P_h from the photon-target rest frame. The angle ψ is the azimuthal angle of ℓ' around the lepton beam axis with respect to an arbitrary fixed direction, which in case of a transversely polarized target we choose to be the direction of S. The corresponding relation between ψ and ϕ_S is given in Ref. [51]; in deep inelastic kinematics one has $d\psi \approx d\phi_S$. The first and second subscript of the above structure functions indicate the respective polarization of beam and target, and if there is a third subscript, it specifies the polarization of the virtual photon.

In theoretical models, the target polarization is defined with respect to the virtual photon momentum direction, however this definition is not practical for experiments. In practice, the target polarization is understood with respect to the incoming electron momentum direction, a frame where the virtual photon has a nonzero transverse momentum. The conversion of the target polarization between the two frames is straightforward [51], and it turns out that measurements with longitudinally polarized targets with respect to the beam receive small contributions from the structure functions with transverse polarization with respect to the photon. Single-hadron measurements indicate that this contribution is usually negligible. This issue will be considered with care in our analysis. For the moment, we restrict our attention only to the longitudinal structure functions.

The relevant spin asymmetries can be built as ratios of structure functions. For the longitudinal polarization of the beam or of the target, denoted with LU and UL, one can define the following asymmetries:

$$\begin{aligned}
A_{LU}^{\sin\phi_R \sin\theta}(x,y,z,M_h,Q) &= \frac{1}{\lambda_e}\,\frac{\frac{8}{\pi}\int d\phi_R\; d\cos\theta\;\; \sin\phi_R\,(d\sigma^+ - d\sigma^-)}{\int d\phi_R\; d\cos\theta\,(d\sigma^+ + d\sigma^-)} = \frac{\frac{4}{\pi}\sqrt{2\,\varepsilon(1-\varepsilon)}\int d\cos\theta\, F_{LU}^{\sin\phi_R}}{\int d\cos\theta\;(F_{UU,T} + \epsilon F_{UU,L})}, \\
A_{UL}^{\sin\phi_R \sin\theta}(x,y,z,M_h,Q) &= \frac{1}{S_L}\,\frac{\frac{8}{\pi}\int d\phi_R\; d\cos\theta\;\; \sin\phi_R\,(d\sigma^+ - d\sigma^-)}{\int d\phi_R\; d\cos\theta\,(d\sigma^+ + d\sigma^-)} = \frac{\frac{4}{\pi}\sqrt{2\,\varepsilon(1+\varepsilon)}\int d\cos\theta\, F_{UL}^{\sin\phi_R}}{\int d\cos\theta\;(F_{UU,T} + \epsilon F_{UU,L})}.
\end{aligned} \tag{4}$$

In particular, this is the $\sin\phi_R$ moment of the asymmetry. The beam spin asymmetry A_{LU} requires a polarized beam and an unpolarized target; if the target is polarized, data sets with each target polarization are combined, for an effectively unpolarized target. The target spin asymmetry A_{UL} requires a longitudinally polarized target, and sums over the electron helicity states. Requiring both a polarized beam and polarized target, the double spin asymmetry A_{LL} is also of interest and similarly defined.

In the $M_h^2 \ll Q^2$ limit[3] the structure functions can be written in terms of PDF and Dihadron Fragmen-

---

[2] From the theoretical point of view, different definitions for the azimuthal angles may be adopted, as long as they differ by terms of order γ^2.

[3] For some discussion of the case of larger M_h, see Ref. [52]

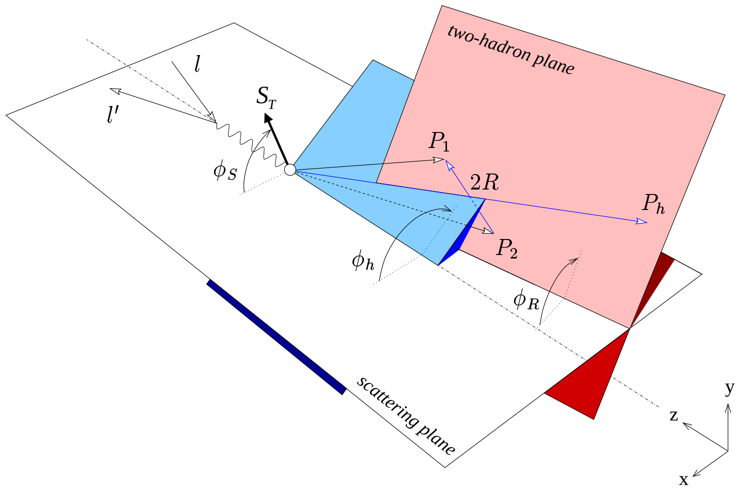

FIG. 1. Definitions of azimuthal angles ϕ_h, ϕ_R, and ϕ_S. The white plane is the lepton scattering plane, the red plane is the plane spanned by the virtual photon and the dihadron total momentum, and the blue plane contains the hadron momenta. From [41].

tation Functions (DiFF) in the following way [42][4]:

$$F_{UU,T} = x f_1^q(x)\, D_1^q\big(z, \cos\theta, M_h\big), \tag{5}$$

$$F_{UU,L} = 0, \tag{6}$$

$$F_{UU}^{\cos\phi_R} = -x \frac{|\boldsymbol{R}|\sin\theta}{Q}\, \frac{1}{z}\, f_1^q(x)\, \widetilde{D}^{\sphericalangle\, q}\big(z, \cos\theta, M_h\big), \tag{7}$$

$$F_{UU}^{\cos 2\phi_R} = 0, \tag{8}$$

$$F_{LU}^{\sin\phi_R} = -x \frac{|\boldsymbol{R}|\sin\theta}{Q} \left[\frac{M}{M_h}\, x\, e^q(x)\, H_1^{\sphericalangle\, q}\big(z, \cos\theta, M_h\big) + \frac{1}{z}\, f_1^q(x)\, \widetilde{G}^{\sphericalangle\, q}\big(z, \cos\theta, M_h\big)\right], \tag{9}$$

$$F_{UL}^{\sin\phi_R} = -x \frac{|\boldsymbol{R}|\sin\theta}{Q} \left[\frac{M}{M_h}\, x\, h_L^q(x)\, H_1^{\sphericalangle\, q}\big(z, \cos\theta, M_h\big) + \frac{1}{z}\, g_1^q(x)\, \widetilde{G}^{\sphericalangle\, q}\big(z, \cos\theta, M_h\big)\right], \tag{10}$$

$$F_{UL}^{\sin 2\phi_R} = 0, \tag{11}$$

$$F_{LL} = x g_1^q(x)\, D_1^q\big(z, \cos\theta, M_h\big), \tag{12}$$

$$F_{LL}^{\cos\phi_R} = -x \frac{|\boldsymbol{R}|\sin\theta}{Q}\, \frac{1}{z}\, g_1^q(x)\, \widetilde{D}^{\sphericalangle\, q}\big(z, \cos\theta, M_h\big), \tag{13}$$

where

$$|\boldsymbol{R}| = \frac{1}{2}\sqrt{M_h^2 - 2(M_1^2 + M_2^2) + (M_1^2 - M_2^2)^2/M_h^2}. \tag{14}$$

All the structure functions that vanish can be nonzero at order $\mathcal{O}\Big(\frac{M^2}{Q^2}, \frac{M_h^2}{Q^2}\Big)$. In the above structure functions, there are essentially three kinds of combinations of PDF and fragmentation functions (FF):[5]

---

[4] a summation $\sum_q e_q^2$ is understood, and the $\vec{k}_T$-integrated T-odd twist-3 distribution functions $h(x)$ and $e_L(x)$ are omitted, which are expected to vanish if the only source of the T-odd behavior is the gauge link

[5] leading-twist functions are always indicated by a subscript 1

leading-twist PDF and FF (e.g., $f_1 D_1$), leading-twist PDF and subleading-twist FF (e.g., $f_1 \widetilde{D}^{\sphericalangle}$), subleading-twist PDF and leading-twist FF (e.g., $e H_1^{\sphericalangle}$).

The main interest of the structure functions with leading-twist combinations ($F_{UU,T}$ in particular) is to allow a flavor-dependent analysis of the DiFF D_1, similarly to what happens for the single-hadron case.

The subleading-twist fragmentation functions $\widetilde{D}^{\sphericalangle}$ and $\widetilde{G}^{\sphericalangle}$ originate from quark-gluon correlation functions on the fragmentation side. They vanish in the so-called Wandzura–Wilczek approximation [53]. Although this approximation is often used in phenomenological works (see, e.g., [54–57] and references therein) there are no compelling theoretical grounds for supporting its validity [58–61]. At present it is neither confirmed nor disproved by experimental data [61]. The measurement of $\cos\phi_R$ modulations in unpolarized or doubly polarized collisions ($F_{UU}^{\cos\phi_R}$ and $F_{LL}^{\cos\phi_R}$) offers a way to address this question directly and represents an example of how dihadron measurements can be useful for the study of quark-gluon correlations in general.

The most interesting terms for our purposes are the ones containing the functions e and h_L, multiplied by the interference fragmentation function $H_1^{\sphericalangle}$, occurring in the structure functions $F_{LU}^{\sin\phi_R}$ and $F_{UL}^{\sin\phi_R}$. The extraction of the PDF is made possible by the fact that $H_1^{\sphericalangle}$ has been extracted [45] from Belle measurements [62]. Unfortunately, the structure functions contain also another term involving the twist-3 fragmentation function $\widetilde{G}^{\sphericalangle}$, although a spectator model calculation [63] predicts its magnitude to be small, except perhaps at low x or high M_h. Measuring the double-spin asymmetry $A_{LL}^{\cos\phi_R}$ as well as evaluating the z and M_h-dependence of the ratio $A_{LU}^{\sin\phi_R}/A_{UL}^{\sin\phi_R}$ can help evaluate the relative magnitude of $\widetilde{G}^{\sphericalangle}$ [3, 64, 65].

C. Partial-wave analysis

Two-hadron fragmentation functions can be decomposed in partial waves in the following way [41, 42]:

$$D_1 \to D_{1,ss+pp} + D_{1,sp}\cos\theta + D_{1,pp}\frac{1}{4}\left(3\cos^2\theta - 1\right), \tag{15}$$

$$G_1^{\perp} \to G_{1,sp}^{\perp} + G_{1,pp}^{\perp}\cos\theta, \tag{16}$$

$$H_1^{\sphericalangle} \to H_{1,sp}^{\sphericalangle} + H_{1,pp}^{\sphericalangle}\cos\theta, \tag{17}$$

$$\widetilde{D}^{\sphericalangle} \to \widetilde{D}_{sp}^{\sphericalangle} + \widetilde{D}_{pp}^{\sphericalangle}\cos\theta, \tag{18}$$

$$\widetilde{G}^{\sphericalangle} \to \widetilde{G}_{sp}^{\sphericalangle} + \widetilde{G}_{pp}^{\sphericalangle}\cos\theta, \tag{19}$$

where the relative partial waves of each pion pair are put into evidence. For sake of simplicity, we will make the replacement $D_{1,ss+pp} \equiv D_1$ since no ambiguity arises in the following. A thorough study of the cross section with partial-wave analysis has been recently presented in Ref. [48], with a different notation compared to the one adopted here. The functions on the r.h.s. depend on z and M_h. It may be useful to note that a symmetrization $f(\theta) + f(\pi - \theta)$ gets rid of all the $\cos\theta$ terms [66]. In general, those terms will vanish even if the θ acceptance is not complete but still symmetric about $\theta = \pi/2$.

Measuring asymmetry modulations in θ enable the ability to constrain the DiFF partial waves. In the full generalization of [48], the DiFF partial waves are associated with angular momentum eigenvalues $\ell = 0, 1, 2$ and $m = -\ell, \ldots, \ell$. Each partial wave term corresponds to a particular interference between two dihadrons which are either in the s-wave or p-wave: a dihadron in the s-wave is unpolarized, whereas one in the p-wave has pseudovector polarization, decomposed into longitudinal and transverse components. The partial wave with $\ell = 0$ corresponds to the interference of two s-wave dihadrons, $\ell = 1$ corresponds to the interference of an s-wave dihadron with a p-wave dihadron, and $\ell = 2$ corresponds to the interference between two p-wave dihadrons. The value of m enumerates the possible relative polarizations of the two dihadrons for each fixed value of ℓ. Consequently, measuring θ-modulations of asymmetries grants access to correlations between the fragmenting quark spin and the angular momentum of the final dihadron state. Understanding such correlations can help shed light on production mechanisms for dihadrons with a specific angular momentum, such as those which originate from the decay of the ρ, a vector meson.

D. Flavor structure

We now discuss the flavor structure of the structure functions. The analysis will be different depending on the kind of target and final-state hadrons. We will consider here $\pi^+\pi^-$, K^+K^-, or $K^+\pi^-$ final-state pairs. Isospin symmetry and charge conjugation suggest the the following relations [45]:

$$D_1^{u\to\pi^+\pi^-} = D_1^{d\to\pi^+\pi^-} = D_1^{\bar{u}\to\pi^+\pi^-} = D_1^{\bar{d}\to\pi^+\pi^-} \ , \tag{20}$$

$$D_1^{s\to\pi^+\pi^-} = D_1^{\bar{s}\to\pi^+\pi^-} \ , \tag{21}$$

$$D_1^{c\to\pi^+\pi^-} = D_1^{\bar{c}\to\pi^+\pi^-} \ , \tag{22}$$

$$H_1^{\sphericalangle u\to\pi^+\pi^-} = -H_1^{\sphericalangle d\to\pi^+\pi^-} = -H_1^{\sphericalangle \bar{u}\to\pi^+\pi^-} = H_1^{\sphericalangle \bar{d}\to\pi^+\pi^-} \ , \tag{23}$$

$$H_1^{\sphericalangle s\to\pi^+\pi^-} = -H_1^{\sphericalangle \bar{s}\to\pi^+\pi^-} = H_1^{\sphericalangle c\to\pi^+\pi^-} = -H_1^{\sphericalangle \bar{c}\to\pi^+\pi^-} = 0 \ . \tag{24}$$

For $\widetilde{G}^{\sphericalangle}$ we expect the same relations as for $H_1^{\sphericalangle}$. In practice, for $\pi^+\pi^-$ and neglecting charm quarks, there are only two independent D_1 functions and one $H_1^{\sphericalangle}$ (and $\widetilde{G}^{\sphericalangle}$).

For dihadrons involving kaons, similar considerations will lead to similar sets of independent dihadron fragmentation functions. For example, the K^+K^- channel has the following relations:

$$D_1^{u\to K^+K^-} = D_1^{\bar{u}\to K^+K^-} , \tag{25}$$

$$D_1^{s\to K^+K^-} = D_1^{\bar{s}\to K^+K^-} \ , \tag{26}$$

$$D_1^{d\to K^+K^-} = D_1^{\bar{d}\to K^+K^-} \ , \tag{27}$$

$$D_1^{c\to K^+K^-} = D_1^{\bar{c}\to K^+K^-} \ , \tag{28}$$

$$H_1^{\sphericalangle u\to K^+K^-} = -H_1^{\sphericalangle \bar{u}\to K^+K^-} \tag{29}$$

$$H_1^{\sphericalangle s\to K^+K^-} = -H_1^{\sphericalangle \bar{s}\to K^+K^-} \ , \tag{30}$$

$$H_1^{\sphericalangle d\to K^+K^-} = -H_1^{\sphericalangle \bar{d}\to K^+K^-} = H_1^{\sphericalangle c\to K^+K^-} = -H_1^{\sphericalangle \bar{c}\to K^+K^-} = 0 \ . \tag{31}$$

Thus, neglecting charm quarks, there are three independent D_1 functions and two $H_1^{\sphericalangle}$ functions, for the K^+K^- channel.

E. Cross sections

Using the expressions of the structure functions (9), and (10), along with the partial-wave expansion of the fragmentation functions in section II C, we can rewrite the asymmetries of equation 4 as

$$A_{LU}^{\sin\phi_R \sin\theta}(x,y,z,M_h,Q) = -\frac{W(y)}{A(y)}\,\frac{M}{Q}\,\frac{|\boldsymbol{R}|}{M_h}\,\frac{\sum_q e_q^2\left[x e^q(x)\,H_{1,sp}^{\sphericalangle,q}(z,M_h) + \frac{M_h}{zM}\,f_1^q(x)\,\widetilde{G}_{sp}^{\sphericalangle,q}(z,M_h)\right]}{\sum_q e_q^2\,f_1^q(x)\,D_1^q(z,M_h)} \ , \tag{32}$$

$$A_{UL}^{\sin\phi_R \sin\theta}(x,y,z,M_h,Q) = -\frac{V(y)}{A(y)}\,\frac{M}{Q}\,\frac{|\boldsymbol{R}|}{M_h}\,\frac{\sum_q e_q^2\left[x h_L^q(x)\,H_{1,sp}^{\sphericalangle,q}(z,M_h) + \frac{M_h}{zM}\,g_1^q(x)\,\widetilde{G}_{sp}^{\sphericalangle,q}(z,M_h)\right]}{\sum_q e_q^2\,f_1^q(x)\,D_1^q(z,M_h)} \ . \tag{33}$$

For the specific case of the $\pi^+\pi^-$ final state, we can introduce in the flavor sum the assumptions (20)–(24), and we get

$$A_{LU}^{\sin\phi_R\sin\theta}(x,y,z,M_h,Q) \approx -\frac{W(y)}{A(y)}\,\frac{M}{Q}\,\frac{|\boldsymbol{R}|}{M_h} \times \frac{H_{1,sp}^{\triangleleft,u}\left[4xe^{u-\bar{u}}(x) - xe^{d-\bar{d}}(x)\right] + \frac{M_h}{zM}\,\widetilde{G}_{sp}^{\triangleleft,u}\left[4f_1^{u-\bar{u}}(x) - f_1^{d-\bar{d}}(x)\right]}{D_1^u\left[4f_1^{u+\bar{u}}(x) + f_1^{d+\bar{d}}(x)\right] + D_1^s\,f_1^{s+\bar{s}}(x)}\,, \tag{34}$$

$$A_{UL}^{\sin\phi_R\sin\theta}(x,y,z,M_h,Q) \approx -\frac{V(y)}{A(y)}\,\frac{M}{Q}\,\frac{|\boldsymbol{R}|}{M_h} \times \frac{H_{1,sp}^{\triangleleft,u}\left[4xh_L^{u-\bar{u}}(x) - xh_L^{d-\bar{d}}(x)\right] + \frac{M_h}{zM}\,\widetilde{G}_{sp}^{\triangleleft,u}\left[4g_1^{u-\bar{u}}(x) - g_1^{d-\bar{d}}(x)\right]}{D_1^u\left[4f_1^{u+\bar{u}}(x) + f_1^{d+\bar{d}}(x)\right] + D_1^s\,f_1^{s+\bar{s}}(x)}\,, \tag{35}$$

where for the PDF we adopt the compact notation $f_1^{q\pm\bar{q}}(x) = f_1^q(x) \pm f_1^{\bar{q}}(x)$, and similarly for the other functions. For neutron targets, assuming isospin symmetry, we can simply interchange the role of u and d quarks in the PDF.

The ratio of beam spin to target spin asymmetries may shed some light on the relative contribution of $\widetilde{G}^{\triangleleft}$:

$$\frac{A_{LU}^{\sin\phi_R\sin\theta}}{A_{UL}^{\sin\phi_R\sin\theta}} = \frac{W(y)}{V(y)}\,\frac{H_{1,sp}^{\triangleleft,u}\left[4e^{u-\bar{u}}(x) - e^{d-\bar{d}}(x)\right] + \frac{M_h}{zM}\widetilde{G}_{sp}^{\triangleleft,u}\left[4f_1^{u-\bar{u}}(x) - f_1^{d-\bar{d}}(x)\right]}{H_{1,sp}^{\triangleleft,u}\left[4h_L^{u-\bar{u}}(x) - h_L^{d-\bar{d}}(x)\right] + \frac{M_h}{zM}\widetilde{G}_{sp}^{\triangleleft,u}\left[4g_1^{u-\bar{u}}(x) - g_1^{d-\bar{d}}(x)\right]}. \tag{36}$$

If $\widetilde{G}_{sp}^{\triangleleft,u}$ is negligible, this ratio simplifies to

$$\frac{A_{LU}^{\sin\phi_R\sin\theta}}{A_{UL}^{\sin\phi_R\sin\theta}} = \frac{W(y)}{V(y)}\,\frac{4e^{u-\bar{u}}(x) - e^{d-\bar{d}}(x)}{4h_L^{u-\bar{u}}(x) - h_L^{d-\bar{d}}(x)}, \tag{37}$$

which is not dependent on z or M_h. Thus if $\widetilde{G}_{sp}^{\triangleleft,u}$ is zero, we expect the asymmetry ratio to be constant in z and M_h [65]; while the converse of this claim may not necessarily be true, the observation of z and/or M_h dependence of this ratio could hint at a non-neglibible contribution from $\widetilde{G}^{\triangleleft}$.

F. Parametrization of the DiFF $H_1^{\triangleleft}$

The chiral-odd Dihadron Fragmentation Function $H_1^{\triangleleft\,q}$ [40] describes the correlation between the transverse polarization of the fragmenting quark with flavor q and the azimuthal orientation of the plane containing the momenta of the detected hadron pair. $H_{1,sp}^{\triangleleft q}$ is the component of $H_1^{\triangleleft q}$ that is sensitive to the interference between the fragmentation amplitudes into pion pairs in relative s wave and in relative p wave, from which comes the common name of Interference Fragmentation Functions [38]. For this reason, we expect the function to be sizeable in kinematic regions where s and p waves are present. This is typically true where spin-1 resonances (e.g., ρ or K^*) are present.

Before the Belle measurement of the angular distribution of two pion pairs in e^+e^- annihilation [62], the only estimates of DiFF were based on model calculations [40, 43, 67]. The unpolarized D_1 was tuned to Monte Carlo event generators [43] and the polarized $H_{1,sp}^{\triangleleft}$ compared to HERMES asymmetry data [68].

The recent analysis of the so-called Artru–Collins asymmetry [69] by the Belle collaboration gave rise to new parametrization of both D_1 and $H_{1,sp}^{\triangleleft}$ for the production of $\pi^+\pi^-$. The former was parameterized to reproduce the two-hadron yields of the PYTHIA event generator, which is known to give a good description of data. Three main decay channels were considered for $\pi^+\pi^-$: (i) ρ resonance decaying into the two pions, (ii) ω resonance decaying into the two pions, plus the fragmentation into a ω resonance decaying into $\pi^+\pi^-\pi^0$ with π^0 unobserved, (iii) the continuum, i.e. the fragmentation into an "incoherent" $\pi^+\pi^-$ pair. Combining the fit of the asymmetry data with the parametrization of its denominator allowed the extraction of the IFF $H_{1,sp}^{\triangleleft}$ [70].

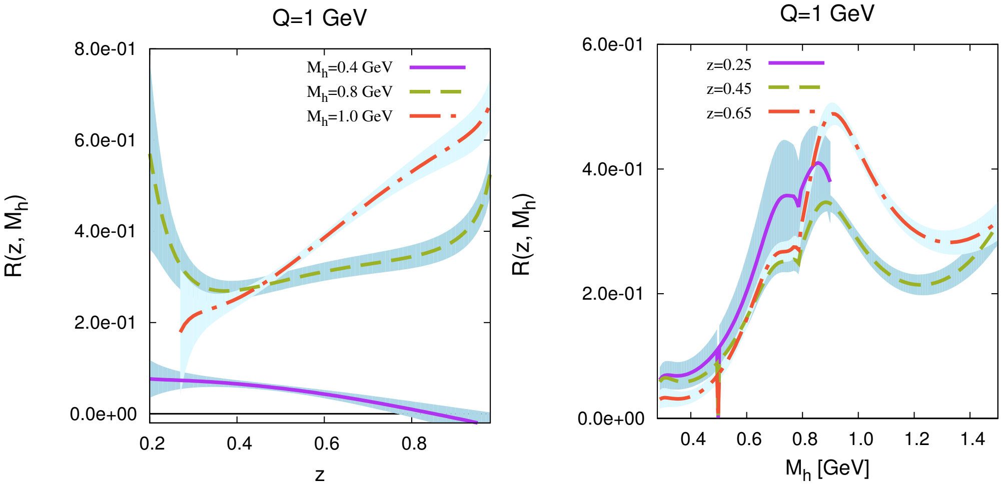

FIG. 2. The ratio $|\boldsymbol{R}|H_{1,sp}^{\triangleleft,u}/M_h D_1^u$ as a function of z and M_h respectively. The error band comes from the calculation of error propagation from the fit.

The ratio $|\boldsymbol{R}|H_{1,sp}^{\triangleleft,u}(z,M_h)/M_h D_1^u(z,M_h)$ at the scale $Q^2 = 1$ GeV^2 is depicted in figure 2. The panels are for the cases integrated over M_h or z, respectively. The error band is estimated through the propagation of errors based on the fit's results.

As an aside, there is at the moment no data on interference fragmentation functions for $K\pi$ pairs. In order to have an estimate of the magnitude of the effect, we assume it to have the form:

$$\frac{|\boldsymbol{R}|H_{1,sp}^{\triangleleft}(z,M_h)}{M_h D_1(z,M_h)} \approx 3M_h \frac{|\boldsymbol{R}|\sqrt{D_{1\mathrm{con}}(z,M_h)\,D_{1K^*}(z,M_h)}}{M_h D_1(z,M_h)}, \tag{38}$$

where with $D_{1\mathrm{con}}$ and D_{1K^*} we mean the components of the fragmentation function that describe the $K\pi$ continuum and the K^* resonance, respectively. We estimate these fragmentation function components using the LEPTO Monte Carlo event generator. The above ansatz is motivated by the fact that the function $H_{1,sp}^{\triangleleft}$ arises from the interference between pairs produced in s wave and p wave (as explained at the beginning of the section). The above ansatz applied to the $\pi^+\pi^-$ system reproduces the size and qualitative feature of the extracted ratio displayed in figure 2. Finally, for $K\pi$ pairs we assume that the fragmentation function is the same for all flavors (the largest component should anyway come from the u quark).

G. Collinear twist-3 parton distribution functions $e(x)$ and $h_L(x)$

The PDFs $e(x)$ and $h_L(x)$ are twist-3 functions which can be decomposed in the following way [20, 49]:

$$xe = x\tilde{e} + \frac{m}{M}\,f_1 + xe_{\mathrm{sing}}, \tag{39}$$

$$xh_L = x\tilde{h}_L + \frac{p_T^2}{M^2}\,h_{1L}^{\perp} + \frac{m}{M}\,g_{1L}. \tag{40}$$

The functions on the left-hand side can be expressed in terms of quark fields only. This property allows an explicit calculation in quark models [71]. The functions with the tilde on the right-hand side are related to quark-gluon-quark correlators and are specifically referred to as "pure twist-3" contributions [58]. The rest of each expression on the right-hand side contains only twist-2 functions, corresponding the Wandzura–Wilczek part. For $e(x)$, there is a term from the unpolarized PDF, along with the local term e_{sing}, which gives rise to a δ-function at $x = 0$. For $h_L(x)$, the wormgear PDF $h_{1L}^{\perp}$ contributes, along with the helicity PDF g_{1L}.

It is insightful to take Mellin moments of $e(x)$ and $h_L(x)$, where the nth Mellin moment a PDF $p(x)$ is given by $\int \mathrm{d}x\, x^{n-1}p(x)$. The first moment of $e(x)$ is proportional to the pion-nucleon sigma-term, which relates to the quark mass contribution to the proton mass (see [20] and references therein), while the second moment

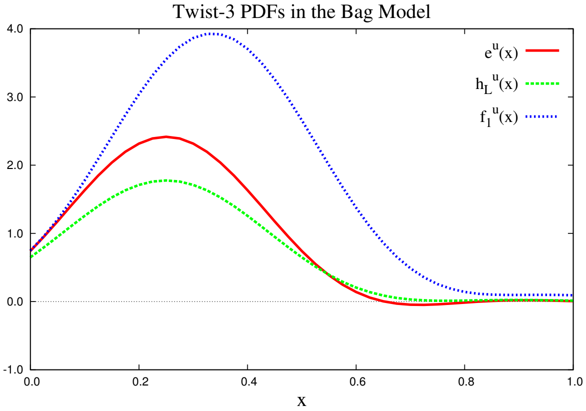

FIG. 3. The functions $e^u(x)$, $h_L^u(x)$, and $f_1^u(x)$ in the bag model [71].

is proportional to the number of valence quarks [64]. The third moment of the twist-3 part of $e(x)$ can be interpreted in deep inelastic scattering as the transverse force acting on the struck quark, immediately after interaction with the virtual photon, with both the quark and parent nucleon having transverse polarization [13].

Regarding Mellin moments of $h_L(x)$, first note that the third moment of the twist-3 part vanishes identically; if it would not vanish, it would correspond analogously to the third moment of $e(x)$, but with the parent nucleon having longitudinal polarization, a scenario which would violate parity [14]. The third moment of $h_L(x)$ only has a twist-2 part, proportional to the third moment of transversity $h_1(x)$. The higher moments of $h_L(x)$ are more interesting, whereas higher moments of $e(x)$ are difficult to interpret. In particular, the fourth moment of the twist-3 part of $h_L(x)$ is related to the average longitudinal gradient of the transverse force acting on transversely polarized quarks; the sign of this gradient provides insights on correlations between the nucleon spin and its color-magnetic field. This moment also can help understand the torque on the struck quark from the color fields, which may provide clues on differences between the Jaffe-Manohar and Ji decompositions of the proton spin [14].

There are a few model calculations concerning the twist-3 PDFs: MIT bag model [71–73], diquark spectator model [74], instanton QCD vacuum calculus [75, 76], chiral quark soliton model [77–81], and the perturbative light-cone Hamiltonian approach to $\mathcal{O}(\alpha_S)$ with a quark target [82, 83]. In these calculations there are no contributions from either strange or sea quarks, except for the chiral quark soliton model.

The bag model has given several powerful results and predictions concerning PDF as well as transverse-momentum dependent distributions (TMD). It is a relativistic model where quarks and antiquarks are excitations inside the confined bag. It is generally assumed that the proton wave function is invariant under the $SU(6)$ spin-flavor symmetry. In the case of two-body problems, this symmetry leads to proportionality between the different flavor components. The contribution to $e(x)$ in the bag is entirely due to the bag boundary, and therefore to the quark-gluon-quark correlation. The result of the model calculation of the twist-3 $e^u(x)$, $h_L^u(x)$, as well as of the unpolarized distribution $f_1^u(x)$, is depicted in figure 3; this can be compared with the chiral quark soliton model, shown in figure 4, which includes additional flavors. On the other hand, the function $h_L(x)$ contains twist-2 and pure twist-3 contributions. Although it is a popular assumption that pure twist-3 (and mass) terms are small [54–57], this has rarely been justified by theoretical calculations.

In the bag model, assuming for simplicity the Wandzura–Wilczek approximation $\widetilde{G}^{\sphericalangle} = 0$, the asymmetries (35) become:

$$A_{LU}^{\sin\phi_R \sin\theta}(x,y,z,M_h,Q) = -\frac{W(y)}{A(y)}\,\frac{M}{Q}\,\frac{|\boldsymbol{R}|}{M_h}\,\frac{\left(4-\frac{1}{2}\right)\,x e^u(x)\,H_{1,sp}^{\sphericalangle,u}(z,M_h)}{\left(4+\frac{1}{2}\right)\,f_1^u(x)\,D_1^u(z,M_h)} \quad , \tag{41}$$

$$A_{UL}^{\sin\phi_R \sin\theta}(x,y,z,M_h,Q) = -\frac{V(y)}{A(y)}\,\frac{M}{Q}\,\frac{|\boldsymbol{R}|}{M_h}\,\frac{\left(4+\frac{1}{4}\right)\,x h_L^u(x)\,H_{1,sp}^{\sphericalangle,u}(z,M_h)}{\left(4+\frac{1}{2}\right)\,f_1^u(x)\,D_1^u(z,M_h)} \quad . \tag{42}$$

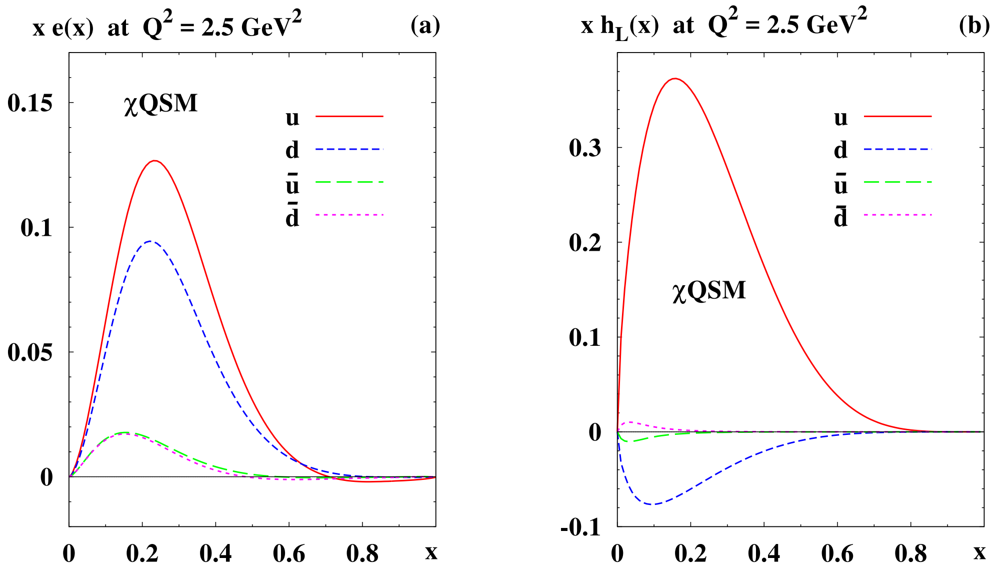

FIG. 4. The parton distribution functions $xe(x)$ and $xh_L(x)$ from the chiral quark soliton model (χQSM) [81, 84]. All results are LO-evolved to $Q^2 = 2.5\,\mathrm{GeV}^2$.

In the spectator model calculation [74], the nucleon states do not strictly follow the $SU(6)$ symmetry and there is no flavor symmetry for a given distribution. Adopting the same approximation as before, in the spectator model the asymmetries (35) become:

$$A_{LU}^{\sin\phi_R \sin\theta}(x, y, z, M_h, Q) = -\frac{W(y)}{A(y)} \frac{M}{Q} \frac{|\boldsymbol{R}|}{M_h} \frac{x\left(4\, e^u(x) - e^d(x)\right)\, H_{1,sp}^{\sphericalangle,u}(z, M_h)}{\left(4\, f_1^u(x) + f_1^d(x)\right)\, D_1^u(z, M_h)} \quad , \tag{43}$$

$$A_{UL}^{\sin\phi_R \sin\theta}(x, y, z, M_h, Q) = -\frac{V(y)}{A(y)} \frac{M}{Q} \frac{|\boldsymbol{R}|}{M_h} \frac{x\left(4\, h_L^u(x) - h_L^d(x)\right)\, H_{1,sp}^{\sphericalangle,u}(z, M_h)}{\left(4\, f_1^u(x) + f_1^d(x)\right)\, D_1^u(z, M_h)} \quad . \tag{44}$$

The results for the twist-3 PDF $e(x)$, $h_L(x)$, and the unpolarized $f_1(x)$ in the spectator model of Ref. [74] are depicted in figure 5 for both the u and d flavor.

In all model results above, the model's scale has been used. This scale turns out to be rather low, $Q_0^2 \sim 0.1$ GeV^2. We neglect the evolution effects on the PDF part of the asymmetries. However, we expect QCD evolution to affect the distributions in pushing them towards lower x values. The missing QCD evolution of the twist-3 PDF is believed to be the largest source of errors in the predictions.

As a final note on twist-3 PDFs, figure 6 shows the first extraction of $e(x)$ [64], based on CLAS6 beam spin asymmetry data. In this figure, the Wandzura-Wilczek approximation is assumed. The higher statistics beam spin asymmetries from CLAS12 will further constrain $e(x)$, while the target spin asymmetries proposed in this document will analogously constrain $h_L(x)$.

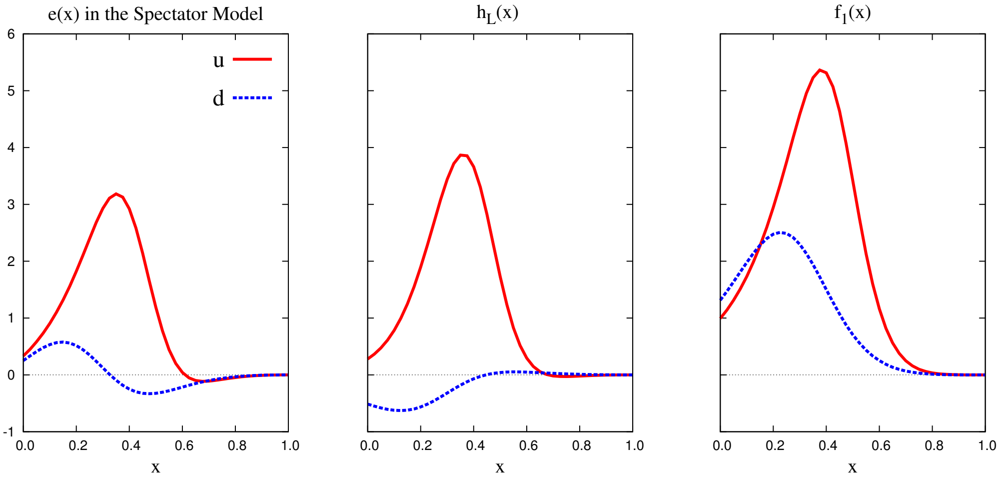

FIG. 5. The function $e^q(x)$, $h_L^q(x)$, $f_1^q(x)$, for $q = u$ (solid red line) and $q = d$ (dotted blue line) in the spectator model of Ref. [74].

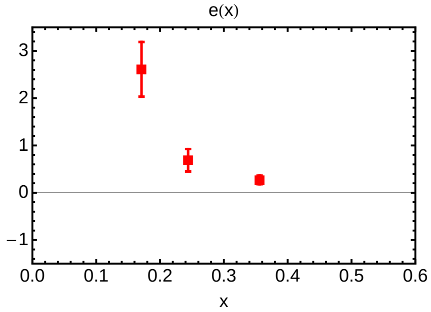

FIG. 6. Extraction of $e^V(x) = 4e^{u_V}(x, Q^2)/9 - e^{d_V}(x, Q^2)/9$ from CLAS6 data. From [64].

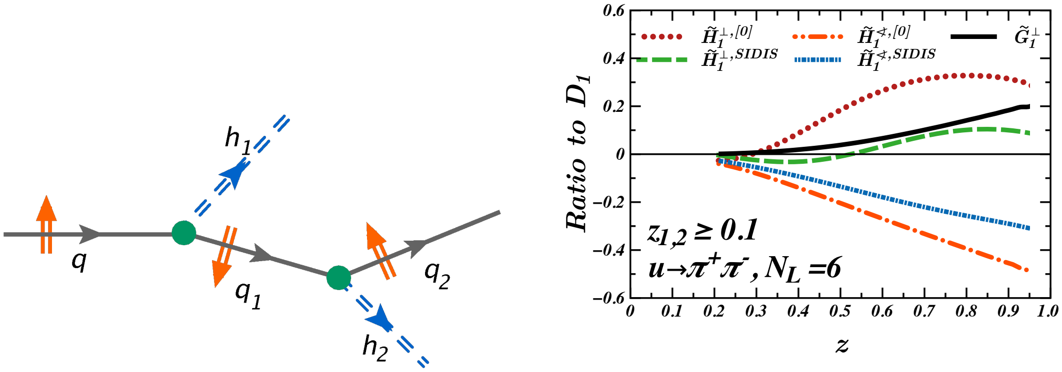

FIG. 7. Hadronization within the quark-jet model including spin (left) and model calculations for the ratios of $G_1^{\perp}$ and $H_1^{\sphericalangle}$ to the unpolarized DiFF D_1 (right). The different definitions for $H_1^{\sphericalangle}$ reflect a process dependence in the definitions for this particular model (e^+e^- versus SIDIS). Here, the $\tilde{H}_1^{\sphericalangle \mathrm{SIDIS}}$ is relevant, where the ˜ denotes that the functions have been integrated over the mass of the dihadron system. Figures taken from [87]

III. Novel spin-orbit correlations in hadronization in DiFFs

As described earlier, having an additional degree of freedom allows the existence of DiFFs that have no correspondence in single-hadron fragmentation. An exciting example is the DiFF $G_1^{\perp}$, which describes the azimuthal dependence of an unpolarized hadron pair on the helicity of the outgoing quark [85]. Similar to, *e*.g., the Boer-Mulders effect, this effect needs intrinsic transverse momentum acquired in the fragmentation process. Fragmentation functions are not accessible on the lattice [2], therefore this channel presents a unique opportunity to extend our knowledge of spin-momentum dynamics in hadronization.

In quark-jet models [86, 87], which describe in the transverse case the observed $H_1^{\sphericalangle}$ well, the intrinsic transverse momentum is acquired in the quark-to-quark splitting in the fragmentation process, and through the associated spin transfer the recoiling quarks acquire a non-zero transverse polarization. These polarizations are correlated, leading to an effect which is predicted to be significant, with the magnitude of $G_1^{\perp}$ about 30% of the magnitude of $H_1^{\sphericalangle}$ [86]. This process, along with the model predictions for $G_1^{\perp}$ compared to $H_1^{\sphericalangle}$, is shown in figure 7. We know that $H_1^{\sphericalangle}$ is large, therefore it is reasonable to expect that we should be able to observe effects sensitive to $G_1^{\perp}$, which is about one third in magnitude.

Another model prediction is from the spectator model [88]. Figure 8 shows the ratio[6] of $G_1^{\perp}$ to the unpolarized DiFF D_1; there is a sign change at the ρ resonance (770 MeV). The authors proceed to extract a corresponding prediction of the target spin asymmetry, which is compared to the COMPASS results from [4]. While the relevant asymmetry measured by COMPASS is consistent with zero within the experimental precision, the spectator model predicts a small asymmetry, which is fairly close to the COMPASS result, as shown in in figure 9.

Aside from the COMPASS results, in the literature there are no constraints on $G_1^{\perp}$ from data. In section VI B we show the recent CLAS12 preliminary result on beam spin asymmetries in dihadron production, which shows promise to provide the first significant constraints. While the analysis is not finalized, it does indicate the presence of a sign change of $G_1^{\perp}$ at the ρ meson mass, consistent with the above spectator model. A longitudinal target would allow for complementary access to $G_1^{\perp}$ through target spin asymmetries, providing further constraints on any extraction.

A. Access to the helicity DiFF

The differential cross section for dihadron production given in equation 2 is integrated over ϕ_h and $P_{h\perp}^2$, causing several terms to vanish. Additional modulations are present if this integration is not performed, the

---

[6] lowest-order partial waves

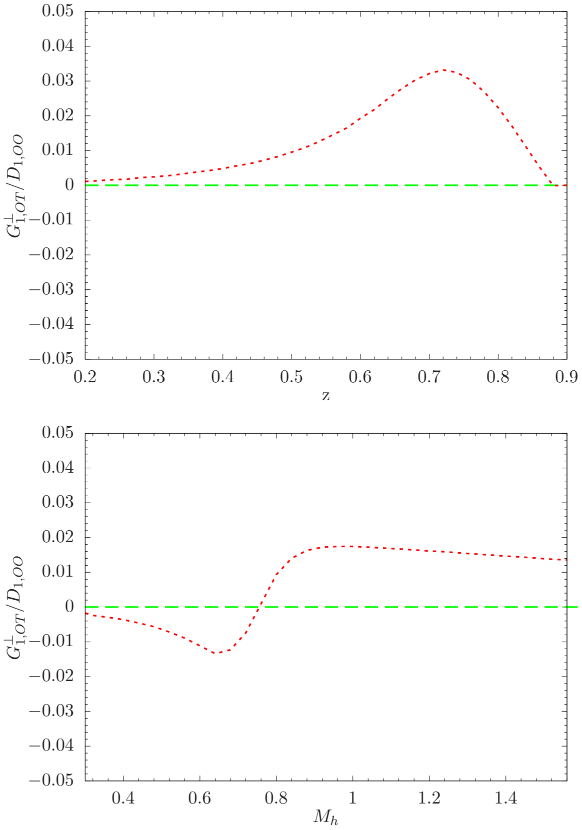

FIG. 8. Spectator model prediction of the ratio $G_{1,OT}^{\perp}/D_{1,OO}$ for z-dependence (left) and M_h-dependence (right). From [88].

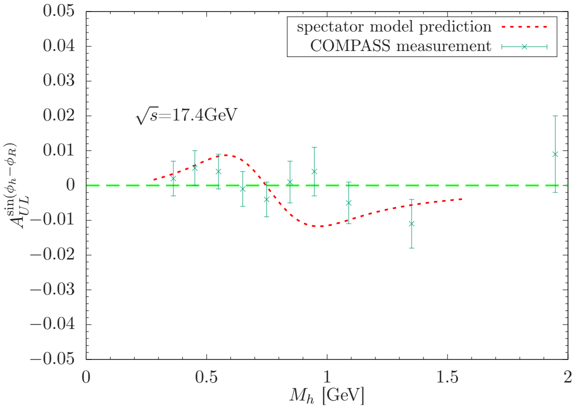

FIG. 9. Spectator model prediction of the target spin asymmetry (dashed curve), compared to the COMPASS result from [4] (points). From [88].

most relevant for this proposal being [48]:

$$F_{LU,T}^{P_{\ell,m}\sin(m(\phi_h-\phi_{R_\perp}))} = -\mathcal{I}\left[2\cos\big(m(\phi_h-\phi_p)\big)f_1G_1^{\perp|\ell,m\rangle}\right]\ , \tag{45}$$

$$F_{UL}^{P_{\ell,m}\sin(m(\phi_h-\phi_{R_\perp}))} = -\mathcal{I}\left[2\cos\big(m(\phi_h-\phi_p)\big)g_{1L}G_1^{\perp|\ell,m\rangle}\right]\ , \tag{46}$$

$$F_{UL}^{P_{\ell,m}\sin((2-m)\phi_h+m\phi_{R_\perp})} = -\mathcal{I}\left[\frac{|\boldsymbol{k}_T||\boldsymbol{p}_T|}{MM_h}\cos\big((m-2)\phi_h+\phi_k+(1-m)\phi_p\big)\,h_{1L}^{\perp}H_1^{\perp|\ell,m\rangle}\right]\ , \tag{47}$$

where $\mathcal{I}$ denotes a weighted convolution of the PDF and FF. The notation $|\ell,m\rangle$ denotes a partial wave of the DiFF, parameterized by angular momentum eigenvalues ℓ and m. The modulations are are expressed as products of a Fourier sinusoid dependent on ϕ_h, ϕ_R, and m, with an associated Legendre polynomial $P_{\ell,m}$ dependent on θ.

The helicity-dependent DiFF $G_1^{\perp}$ is found in equations 45 and 46, and is experimentally accessible via target-spin and beam-spin asymmetries A_{UL} and A_{LU}. In A_{LU} it couples to the spin averaged PDF $f_1(x)$, whereas in A_{UL} it couples to the helicity distribution $g_1(x)$, both of which have a significant magnitude. Additionally, equation 47 shows sensitivity to the wormgear distribution function $h_{1L}^{\perp}$ coupled with the $H_1^{\perp}$ DiFF.

Some of the initial interest in $G_1^{\perp}$ was motivated by its connection to the so-called jet-handedness [85], which in turn might receive contributions from CP-violating QCD vacuum fluctuations [20]. This was one reason for the measurement at Belle [89] which did not find a signal. However, after a revisit of the original calculation by another theory group [90], it became clear this was due to a sign-mistake in the original calculation. For SIDIS, they propose a measurement of dihadron asymmetries with the weight factors [91, 92]:

$$A = \frac{\langle P_{h\perp}\sin(\phi_h-\phi_R)/M_h\rangle}{\langle 1\rangle} = \frac{\int d_{LU}P_{h\perp}\sin(\phi_h-\phi_R)/M_h}{\int d_{UU}}. \tag{48}$$

This weight breaks the convolution of the PDF and DiFF between the initial and final quark transverse momenta, returning a product of the PDF and DiFF; note that the DiFFs (and PDFs) are themselves integrated over the initial quark transverse momentum. The corresponding weighted spin asymmetries are:

$$A_{UL}^{\rightrightarrows}(x,z,M_h^2) = S_L\frac{\sum_a e_a^2\ g_{1L}^a(x)\ z\ G_1^{\perp a}(z,M_h^2)}{\sum_a e_a^2\ f_1^a(x)\ D_1^a(z,M_h^2)}, \tag{49}$$

$$A_{LU}^{\rightrightarrows}(x,y,z,M_h^2) = \lambda_l\frac{C'(y)}{A'(y)}\frac{\sum_a e_a^2\ f_1^a(x)\ z\ G_1^{\perp a}(z,M_h^2)}{\sum_a e_a^2\ f_1^a(x)\ D_1^a(z,M_h^2)}. \tag{50}$$

The aforementioned CLAS12 preliminary result is of this beam spin asymmetry, while the target spin asymmetry is another proposed measurement for the longitudinal target program. A measurement of both is complementary, since each corresponds to a coupling with a different PDF.

This is the first time that a TMD DiFF will be measured, and it can also be accessed in a re-measurement of $G_1^{\perp}$ in e^+e^- annihilation, which is well motivated to test the validity of factorization. A comparison with the SIDIS measurements might be sensitive to parity violating vacuum fluctuations as discussed above.

B. Transverse Momentum Dependent DiFFs

It is interesting to draw analogies between single-hadron TMD FFs, accessible in Λ production, to TMD DiFFs. Table II shows an attempt at a comparison, where the left half is for single-hadron FF and the right half for DiFFs. Dihadron polarization is better understood within the partial wave expansion, however, so it is more correct to expand the matrix to include the interference between relative s and p waves.

To do the expansion, we first enumerate the possible polarization pairings in the interference terms. Truncating the expansion at $\ell = 2$, which limits us to consider only up to a relative p wave difference, the s-state dihadron is unpolarized (denoted U or O), and the p-state dihadron has either transverse (T) or longitudinal (L) polarization; $\ell = 0$ corresponds to the ss terms, $\ell = 1$ to the sp terms, and $\ell = 2$ to the pp terms. We can then rearrange these partial waves into an enhanced table of DiFFs, following the notation given in equations 62-74 of [48]. Table III is the updated table, where rows are grouped by the following classifications:

h/q	**U**	**L**	**T**	**h/q**	**U**	**L**	**T**
U	$D_1^{\Lambda/q}$		$H_1^{\perp,\Lambda/q}$	**U**	$D_1^{h_1h_2/q}$		$H_1^{\perp,h_1h_2/q}$
L		$G_1^{\Lambda/q}$	$H_{1L}^{\Lambda/q\perp}$	**L**			
T	$D_{1T}^{\perp\Lambda/q}$	$G_{1T}^{\perp\Lambda/q}$	$H_1^{\Lambda/q}$,$H_{1T}^{\perp\Lambda/q}$	**T**		$G_1^{\perp h_1h_2/q}$	$H_1^{\triangleleft h_1h_2/q}$

TABLE II. TMD FFs for Λ production (left) and dihadrons (right) appearing at leading order in $^1/_{Q^2}$ in the SIDIS cross section. The U, L, and T labels of the rows (columns) represent the dependence of the distributions on the polarization (unpolarized, longitudinally, transversely) of the quark (hadron).

h_1h_2/q	**U**	**L**	**T**
UU	$D_{1,OO}$		$H_{1,OO}^{\perp}$
LU	$D_{1,OL}$		$H_{1,OL}^{\perp}$
LL	$D_{1,LL}$		$H_{1,LL}^{\perp}$
TU	$D_{1,OT}$	$G_{1,OT}^{\perp}$	$\begin{cases} H_{1,OT}^{\perp} & \text{if } m<0 \\ H_{1,OT}^{\triangleleft} & \text{if } m>0 \end{cases}$
TL	$D_{1,LT}$	$G_{1,LT}^{\perp}$	$\begin{cases} H_{1,LT}^{\perp} & \text{if } m<0 \\ H_{1,LT}^{\triangleleft} & \text{if } m>0 \end{cases}$
TT	$D_{1,TT}$	$G_{1,TT}^{\perp}$	$\begin{cases} H_{1,TT}^{\perp} & \text{if } m<0 \\ H_{1,TT}^{\triangleleft} & \text{if } m>0 \end{cases}$

TABLE III. Table of DiFFs, where the rows are the dihadron polarizations, *i.e.*, interference, and the columns are the fragmenting quark polarization; the DiFFs follow the notation given in [48]

- unpolarized only, the ss terms
- interference with longitudinally polarized dihadron, but not transverse, which contains sp and pp terms with $m = 0$
- interference with transversely polarized dihadron, which contains sp and pp terms with $m = 1, 2$

It is interesting to note that $G_1^{\perp}$ necessitates the interference with a transversely polarized dihadron, while this DiFF encodes a correlation of fragmenting quark with longitudinal polarization; this correlation of longitudinal quark polarization to transverse dihadron polarization could represent a contribution from a "wormgear-like" splitting.

IV. Correlations in hadron production in the current and target fragmentation region

All of the above asymmetries assume the factorization model with the hadron production occurring from the scattered parton, that is, in the Current Fragmentation Region (CFR). It is possible to study hadronization which originates from the target as well, which is called the Target Fragmentation Region (TFR). Correlations between hadrons from the CFR with those from the TFR represent another class of dihadron production which is of interest in this section.

As it has becomes clear during the last decades, the study of the three dimensional spin-dependent partonic structure of the nucleon requires excellent understanding of the hadronization process after hard lepton-quark scattering. The unique feature of CLAS12 is the wide coverage of the produced hadron phase space; in contrast to previous SIDIS experiments, we will have access not only to the CFR but also to the TFR. These two regions are defined in the virtual photon-target nucleon center of mass frame, with the z-axis aligned to the virtual photon momentum. The CFR includes hadrons produced in the forward hemisphere (along the virtual photon), whereas the TFR is for hadrons produced in the backward hemisphere.

The QCD description of this process for collinear kinematics includes new nonperturbative objects, the fracture functions, which were first introduced by Trentadue and Veneziano [46]. Recently this approach was generalized by Anselmino, Barone and Kotzinian [47] to the spin and transverse momentum dependent case. The fracture functions represent the conditional probabilities to find an unpolarized, a longitudinally polarized, or a transversely polarized quark with longitudinal momentum fraction x and transverse momentum $\mathbf{k}$ inside a nucleon, fragmenting into a hadron carrying a fraction $\zeta = P_h^-/P^- \simeq E_h/E$ of the nucleon longitudinal momentum and a transverse momentum $\mathbf{P}_h$.

The general LO cross section expression for SIDIS in the TFR is presented in [47] and gives access only to four quark-transverse-momentum integrated fracture functions. To gain access to all LO fracture functions, one has to "measure" the final quark transverse polarization. The Double SIDIS process, outlined in the next section, allows this by means of the Collins effect for hadrons produced in the CFR. Exploiting SIDIS in TFR, Double SIDIS will allow us to check the validity of factorization and deepen our understanding the hadronization mechanism.

A. The Double SIDIS (DSIDIS) process

Let us consider the polarized SIDIS process in equation 1 with one hadron produced in the current fragmentation region (CFR) and the other in the target fragmentation region (TFR) [93], shown in figure 10. The LO expression for Spin and Transverse Momentum Dependent (STMD) DSIDIS is given as:

$$\frac{d\sigma^{\ell(l,\lambda)+N(P,S)\to\ell(l')+h_1(P_1)+h_2(P_2)+X}}{dx\,dQ^2\,d\phi_S\,dz\,d^2P_{T1}\,d\zeta\,d^2P_{T2}} = \sum_q \mathcal{M}^{h_2}_{q,s/N,S} \otimes \frac{d\sigma^{\ell(l,\lambda)+q(k,s)\to\ell(l')+q(k',s')}}{dQ^2} \otimes D^{h_1}_{q,s'}\,, \tag{51}$$

where $\mathcal{M}^{h_2}_{q,s/N,S}$ are the STMD fracture functions, and $D^{h_1}_{q,s'}$ are the STMD fragmentation functions to a spinless hadron from unpolarized and transversely polarized quarks (see, for example, [49]),

$$D^{h_1}_{q,s'}(z,\mathbf{p}) = D_1(z,p^2) + \frac{\mathbf{p}\times\mathbf{s}'}{m_h} H_1(z,p^2), \tag{52}$$

where $\mathbf{p}$ is a transverse momentum of the hadron, with respect to the fragmenting quark momentum.

The cross section for the DSIDIS from a polarized lepton scattering off a longitudinally polarized nucleon can be written in the form:

$$\frac{d\sigma^{\ell(l,\lambda)+N(P,S)\to\ell(l')+h_1(P_1)+h_2(P_2)+X}}{dx\,dy\,d\phi_S\,dz\,d^2P_{T1}\,d\zeta\,d^2P_{T2}} =$$

$$\frac{\alpha^2\,x}{Q^4 y}\left(1+(1-y)^2\right)\left(\sigma_{UU} + S_L\,\sigma_{UL} + S_T\,\sigma_{UT} + \lambda\,D_{ll}\sigma_{LU} + \lambda\,S_L D_{ll}\,\sigma_{LL} + \lambda\,S_T D_{ll}\,\sigma_{LT}\right)\,, \tag{53}$$

where

$$D_{ll}(y) = \frac{y(2-y)}{1+(1-y)^2}\,. \tag{54}$$

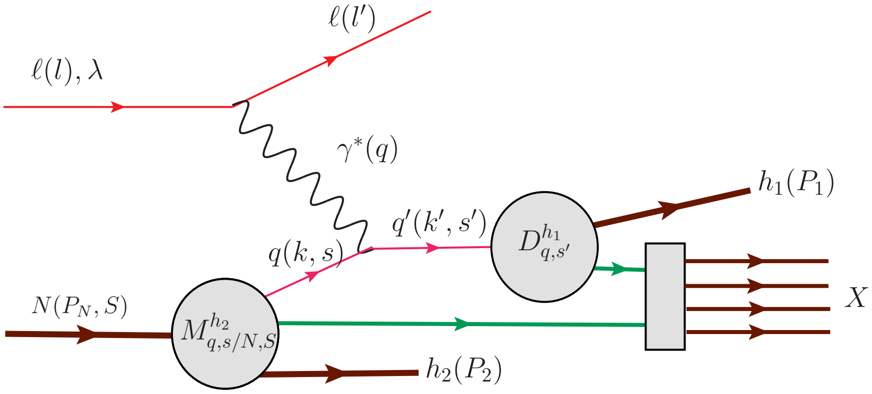

FIG. 10. DSIDIS description with hadronization function. From [93].

The terms depending on the longitudinal polarization of initial particles are given by [94]:

$$\begin{aligned}\sigma_{UU} = F_0^{\hat{M}\cdot D_1} - D_{nn}\Bigg[& \frac{P_{T1}^2}{m_1 m_N}\, F_{kp1}^{\hat{h}_1^{\perp}\cdot H_1}\cos(2\phi_1) \\ & + \frac{P_{T1}P_{T2}}{m_1 m_2}\, F_{p1}^{\hat{h}_1^{h}\cdot H_1}\cos(\phi_1+\phi_2) \\ & + \left(\frac{P_{T2}^2}{m_1 m_N}\, F_{kp2}^{\hat{h}_1^{\perp}\cdot H_1} + \frac{P_{T2}^2}{m_1 m_2}\, F_{p2}^{\hat{h}_1^{h}\cdot H_1}\right)\cos(2\phi_2)\Bigg],\end{aligned} \tag{55}$$

$$\begin{aligned}\sigma_{UL} = & -\frac{P_{T1}P_{T2}}{m_2 m_N}\, F_{k1}^{\hat{M}_L^{\perp h}\cdot D_1}\sin(\phi_1-\phi_2) \\ & + D_{nn}\Bigg[\frac{P_{T1}^2}{m_1 m_N} F_{kp1}^{\hat{h}_{1L}^{\perp}\cdot H_1}\sin(2\phi_1) \\ & + \frac{P_{T1}P_{T2}}{m_1 m_2} F_{p1}^{\hat{h}_{1L}^{h}\cdot H_1}\sin(\phi_1+\phi_2) \\ & + \left(\frac{P_{T2}^2}{m_1 m_N} F_{kp2}^{\hat{h}_{1L}^{\perp}\cdot H_1} + \frac{P_{T2}^2}{m_1 m_2} F_{p2}^{\hat{h}_{1L}^{h}\cdot H_1}\right)\sin(2\phi_2)\Bigg],\end{aligned} \tag{56}$$

$$\sigma_{LU} = -\frac{P_{T1}P_{T2}}{m_2 m_N} F_{k1}^{\hat{g}_1^{\perp h}\cdot D_1}\sin(\phi_1-\phi_2)\,, \tag{57}$$

$$\sigma_{LL} = F_0^{\hat{g}_{1L}\cdot D_1}\,, \tag{58}$$

where

$$D_{nn}(y) = \frac{(1-y)}{1+(1-y)^2}\,. \tag{59}$$

The structure functions $F_0^{\Delta\hat{M}_L\cdot D_1}$, $F_{k1}^{\Delta\hat{M}^{\perp h}\cdot D_1}$, *etc.* are convolutions of the fracture function M and fragmentation function D (see appendix B). For example, we have

$$F_{UU} = \mathcal{C}\big[\check{f}_1 D_1\big], \tag{60}$$

$$F_{UU}^{\cos 2\phi_1} = \mathcal{C}\Big[-\frac{2\,(\hat{\boldsymbol{h}}\cdot\boldsymbol{k}_T)\,(\hat{\boldsymbol{h}}\cdot\boldsymbol{p}_T) - \boldsymbol{k}_T\cdot\boldsymbol{p}_T}{MM_h}\check{h}_1^{\perp}H_1^{\perp}\Big], \tag{61}$$

$$F_{UL}^{\sin 2\phi_1} = \mathcal{C}\Big[-\frac{2\,(\hat{\boldsymbol{h}}\cdot\boldsymbol{k}_T)\,(\hat{\boldsymbol{h}}\cdot\boldsymbol{p}_T) - \boldsymbol{k}_T\cdot\boldsymbol{p}_T}{MM_h}\check{h}_{1L}^{\perp}H_1^{\perp}\Big], \tag{62}$$

$$F_{LL} = \mathcal{C}\big[\check{g}_{1L} D_1\big], \tag{63}$$

where the standard convolution notation

$$\mathcal{C}\big[w\,f\,D\big] = x\sum_a e_a^2\int d^2\boldsymbol{k}\,d^2\boldsymbol{p}\,\delta^{(2)}\big(\boldsymbol{k}-\boldsymbol{p}-\boldsymbol{P}_{h\perp}/z\big)\,w(\boldsymbol{k},\boldsymbol{p})\,f^a(x,\zeta,\boldsymbol{k}^2)\,D^a(z,\boldsymbol{p}^2) \tag{64}$$

was used, the unit vector $\hat{\boldsymbol{h}} = \boldsymbol{P}_{h\perp}/|\boldsymbol{P}_{h\perp}|$, and

$$\check{f}_1(x,\zeta,\mathbf{k}^2) = \int \mathrm{d}^2\mathbf{P}_h\,\hat{f}_1\,, \tag{65}$$

$$\check{g}_{1L}(x,\zeta,\mathbf{k}^2) = \int \mathrm{d}^2\mathbf{P}_h\hat{g}_{1L}\,, \tag{66}$$

$$\check{h}_{1L}^{\perp}(x,\zeta,\mathbf{k}^2) = \int \mathrm{d}^2\mathbf{P}_h\left(\hat{h}_{1L}^{\perp} + \frac{m_N}{m_h}\,\frac{\mathbf{k}\cdot\mathbf{P}_h}{\mathbf{k}^2}\,\hat{h}_{1L}^{h}\right)\,, \tag{67}$$

$$\check{h}_1^{\perp}(x,\zeta,\mathbf{k}^2) = -\int \mathrm{d}^2\mathbf{P}_h\left(\hat{h}_1^{\perp} + \frac{m_N}{m_h}\,\frac{\mathbf{k}\cdot\mathbf{P}_h}{\mathbf{k}^2}\,\hat{h}_1^{h}\right)\,. \tag{68}$$

The fracture functions which depend on quark polarization have the notation $\hat{g}$ for longitudinally polarized quarks and $\hat{h}$ for transversely polarized quarks, whereas $\hat{f}$ corresponds to unpolarized quarks.

Equations 55-58 indicate the various fracture functions that azimuthal modulations of DSIDIS spin asymmetries are sensitive to. Beam spin asymmetries give access only to $\hat{g}_1$, the fracture function of longitudinally polarized quarks in an unpolarized nucleon. With the addition of target polarization, several other fracture functions become accessible in modulations of the target spin and double spin asymmetries:

- $\hat{M}_L$: unpolarized quark in a longitudinally polarized nucleon
- $\hat{h}_{1L}$: transversely polarized quark in a longitudinally polarized nucleon (note there are two types for this case: $\hat{h}_{1L}^h$ which includes a factor of $P_{h\perp}$ and $\hat{h}_{1L}^{\perp}$ which includes a factor of $k_\perp$).
- $\hat{g}_{1L}$: longitudinally polarized quark in a longitudinally polarized nucleon; this one is accessible in the double spin asymmetry

Significant SSAs have been measured by CLAS for azimuthal correlations of hadrons in the target and current fragmentation regions, providing direct access to underlying fracture functions [95]. Figure 11 shows that A_{LU} is very significant at large x, which is the kinematic region of most interest for our proposal.

Finally, we mention the DSIDIS cross section LO expressions can be studied for three different cases: (i) integrated over TFR hadron transverse momentum, (ii) over CFR hadron transverse momentum and (iii) unintegrated over transverse momenta. The expressions are rather simple for (i) and (ii), but experimental measurements of azimuthal asymmetries in these cases will be more difficult since azimuthal acceptance corrections will be needed. In (iii), the three-dimensional (in azimuths) analysis will allow to avoid this problem and will give access to all TMD fracture functions. Measured single and double leading twist asymmetries for pion and kaon pairs in a large range of kinematic variables (x, Q^2, z, $P_{h\perp}$, and ϕ), with longitudinally polarized targets, will thus provide a first glimpse into the fracture functions.

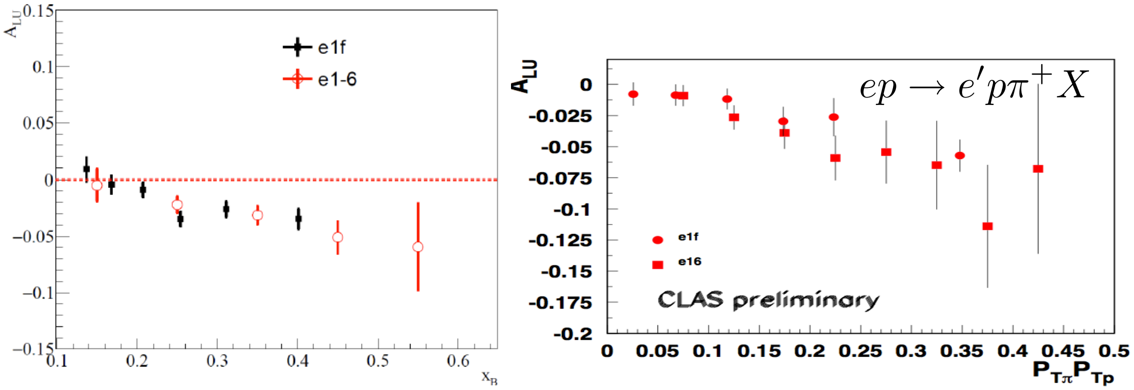

FIG. 11. $A_{LU}^{\sin(\phi_2-\phi_1)}$ dependence on x (left) and on $P_{T_\pi}P_{T_p}$ (right), for the process $ep \to e'p\pi^+X$ with pion $x_F > 0$ and proton $x_F < 0$ and $0.4 < z_\pi < 0.7$. The different point sets correspond to different datasets. From the presentation associated with [95].

V. Experimental details

A. CLAS12

The proposed measurements will be taken simultaneously with the approved CLAS12 experiments for semi-inclusive DIS studies with CLAS12 [7–10], with longitudinally polarized proton and deuteron targets. We will use the upgraded CLAS12 spectrometer [96] with part of the low threshold Cherenkov counter replaced by the ring-imaging Cherenkov detectors, which will help allow for kaon identification. We will run at the standard magnetic field configurations. The central tracker will also be used for coincident detection of protons, pions and kaons both in target and current fragmentation regions. The solenoid for the central tracker is also used simultaneously to provide the magnetic field for the polarized target.

B. CLAS12 Particle Identification

In the baseline design of CLAS12 [96, 97], particle identification (PID) in the forward detector is obtained by using a high threshold Cerenkov counter (HTCC) [98], a low threshold Cerenkov counter (LTCC) [99], and time-of-flight scintillator arrays (TOF) [100, 101]. In the ∼2.5–5 GeV/c momentum region, the kaon-pion separation relies only on the LTCC performance, and it is not possible to separate protons from kaons in the 4.7–8 GeV/c momentum region. While, in general, this PID system matches the requirements of the physics program at 12 GeV, it turns out to be insufficient for some physics reactions of high interest, such as the ones covered by this proposal that require charged kaon detection. More specifically, since the K/π production ratio is of the order of 10–15% (see figure 12), a very high rejection factor for pions is needed in order to keep the contamination of misidentified kaons at a few percent level, while, with the baseline configuration and assuming a 10% pion detection inefficiency for the LTCC, the π/K contamination is 1:1.

An improved hadron PID is therefore needed, which can be achieved with a Ring Imaging Cherenkov (RICH) detector. Currently, one of the CLAS sectors (out of 6) is covered by a new RICH detector [102], which has been installed in place of the LTCC. The RICH ensures a 1:500 rejection factor for pions, corresponding to a 4σ pion-kaon separation in the 3–8 GeV/c momentum range. A second RICH sector, currently under construction, is planned to be ready by the time of the proposed run period. With the two RICH detectors in operation, installed in opposite sectors, it will be possible to meet the PID performances needed for SIDIS dihadron measurements with πK and KK final states where the kaon has large momentum. Note that since in the dihadron channel the momentum is shared between the outgoing hadrons, one of the hadrons usually has a low enough momentum to be discriminated with the CLAS12 baseline PID detectors (*i.e.*, without the RICH).

C. The polarized target

The target configuration will be that of the approved experiments using the polarized target [7–10]. Further information on the target design can be found in [103–105]. The targets will be polarized via the method of Dynamic Nuclear Polarization (DNP), which is a well established technique that has been used extensively in nuclear and particle physics experiments, including the ones performed in Hall B of Jefferson Lab. Dynamically polarized target systems consist of a hydrogenated (polarized protons) or deuterated (polarized neutrons) compound containing paramagnetic centers, such as unpaired electrons, placed in a high magnetic field and cooled to low temperatures, with a B/T ratio of the order of 5 Tesla/Kelvin. In these conditions, the free electron spins can approach polarization of 100%. The high polarization of unpaired electrons is then transferred dynamically to the nucleons by irradiating the target material at frequency near that of electron spin resonance. This technique typically allows to achieve a proton polarization of 80–90%, and a deuteron polarization of 30–40%. The nucleons in the target will be polarized either parallel or anti-parallel to the electron beam direction.

The main systems required to realize DNP are a superconducting magnet, a ^{4}He evaporation refrigerator to maintain the target material at 1 K, a target insert, which will house the target material and some additional instrumentation, a microwave system to transfer the polarization to the nucleon spins, and a

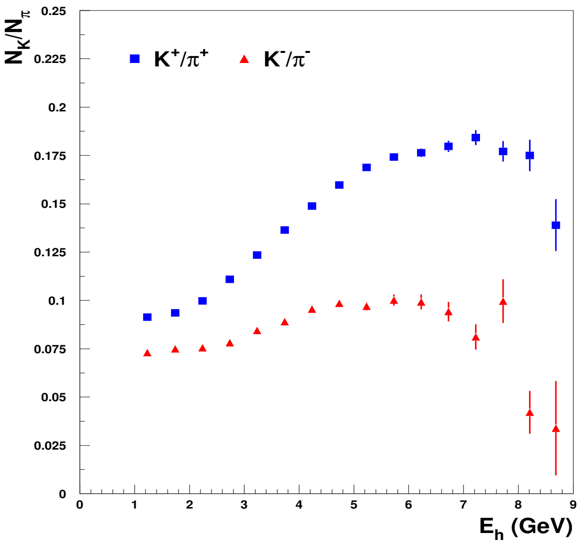

FIG. 12. Semi-Inclusive kaon versus pion yield ratio.

Nuclear Magnetic Resonance (NMR) system to determine the state of polarization.

In CLAS12 the polarizing magnetic field will be provided by the superconducting solenoid of the central detector. Ammonia (NH_3) and deuterated ammonia (ND_3) will be used as target materials. In order to determine the dilution factor (fraction of events originating from polarized target materials) for each process with sufficiently high accuracy, about 20% of the running time will be devoted to measurements with carbon, nitrogen, and helium. To determine the proton to deuteron and deuteron to carbon cross section ratios, we will need a few days of running with the same magnetic fields and target position as the present experiment, but with gas or liquid hydrogen and deuterium targets. We anticipate that this can be scheduled in conjunction with other planned experiments with CLAS12.

For measurements on polarized deuterium, while we plan to use the ND_3 target, we could also make use of the ^{3}He target, which is also proposed to this year's PAC [106] (see also [107]). The ^{3}He target has similar dilution, but a higher polarization of 50%. With a higher polarization statistical uncertainties will be lower; moreover, having two different targets could lead to a better understanding of systematics. It would be most advantageous to make use of data from both targets for a full analysis with polarized deuterium.

The target polarization will be monitored during the run via the NMR system, in the field of the solenoid magnet [108]. The calibration of the proton NMR can be done by measurements of polarization in thermal equilibrium, taken with the polarizing magnet. The experiment will run with a beam of about 10 nA on a 5 cm long ammonia target, resulting in a luminosity of $10^{35}/\text{cm}^2\text{s}$. The beam will be rastered over the diameter of the polarized target to minimize the dose density (we will need at most one anneal every other day under these conditions).

D. The data set and analysis

The expected kinematical coverage in the DIS region with an 11 GeV beam at CLAS12 is shown in figure 13. This coverage constitutes a substantial increase over the existing CLAS6 data in both x and Q^2, while the precision of the expected data in the valence region will be far superior to existing DIS experiments from other labs.

Realistic MC simulations are crucial for separation of different contributions to azimuthal moments arising from higher twists, both kinematical [109] and dynamical [110–113], radiative corrections [114, 115] and in particular from the detector acceptance. The CLAS12 FAST-MC program was used to simulate the physics events and study the extraction of azimuthal moments and acceptance corrections. The large acceptance of

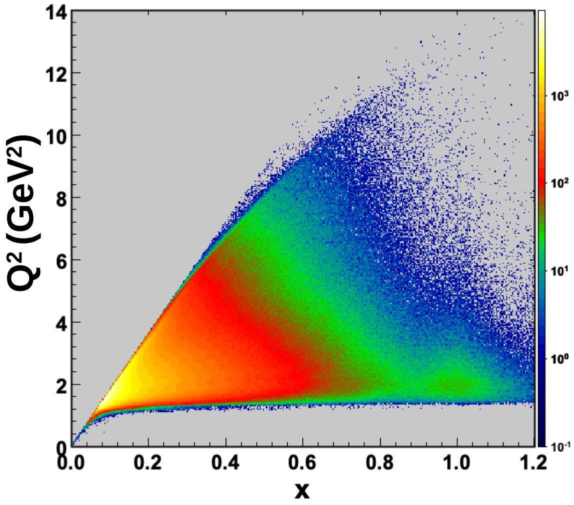

FIG. 13. Kinematical coverage at CLAS12.

CLAS12 allows detection of final state hadrons produced both in target and current fragmentation regions. The 2D x_F-distributions are shown on figure 14. By selecting different kinematical regions, one can measure azimuthal asymmetries in those regions and extract underlying non-perturbative functions.

Figure 15 shows the typical mass distribution for $\pi^+\pi^-$ dihadron production, along with contributions from various meson decay channels. The CLAS12 data occupy the same region shown on the figure. In particular there is a large contribution from ρ-mesons, which can be selected by a cut on M_h and additionally on the angular momentum from a partial wave analysis. Because such a large fraction of pions can originate from a ρ decay, understanding the ρ production mechanism from the perspective of dihadrons can help clarify single pion production.

In projected results we assume a beam polarization of 0.8, which has been routinely achieved in recent experiments running at Jefferson Lab. The beam helicity will be flipped in a pseudo-random pattern every 33 ms. We will use the standard Hall B beam devices to monitor and stabilize the beam intensity and position. In particular, we will reduce any helicity-correlated beam asymmetries to less than 10^{-3}.

The data will consist of the number of counts for beam electron or target proton helicity parallel (N^+) and anti-parallel (N^-) states, each normalized to the dead-time corrected integrated beam charge; details of the trigger system are found at [116]. We will subtract from these rates the backgrounds from misidentified kaons/pions (which can be obtained from fits to the distribution of photo-electrons in the high-threshold Cerenkov counter and the measured ratio of visible energy deposited in the electromagnetic calorimeter to the measured momentum) and from electrons coming from pair-symmetric decays (e.g., $\pi^0 \to e^+e^-$ or $\pi^0 \to \gamma e^+e^-$ as well as $\gamma \to e^+e^-$ conversions). From the corrected counts, we will form the ratio $A^{raw} = (N^+ - N^-)/(N^+ + N^-)$. This ratio is "raw" in the sense that it has to be divided by the target polarization and the dilution factor.

For the polarized target configuration, following the procedure developed for the single-hadron case [10], the dilution factor can be calculated from a detailed model of the target content. The only ingredient needed is the packing fraction (the fraction of the cell volume occupied by the ammonia beads), which can be extracted by comparing the rate from ammonia to that from an auxiliary carbon target. Additional measurements on empty and liquid-helium only targets will also be needed. Past experience with the EG1 experiment in Hall B has shown that a typical error of 3% on the dilution factor can be achieved [117]. An additional correction for the small polarization in ^{15}N and contamination by ^{14}N and, in the case of the deuterated ammonia, H, will be applied as well. Section VI C includes some plots that show the dependence of dilution factors on kinematic variables.

The beam (P_B) and target (P_T) polarization will be independently measured using Möller scattering and NMR, respectively. The target polarization, however, can be extracted from the product of $P_B * P_T$ with higher precision directly from our data, by measuring the asymmetry of elastic (quasi-elastic) scattering $\vec{p}(\vec{e}, e'p)$ ($\vec{d}(\vec{e}, e'p)$) from our NH_3 (ND_3) targets, respectively. We did a full simulation of this

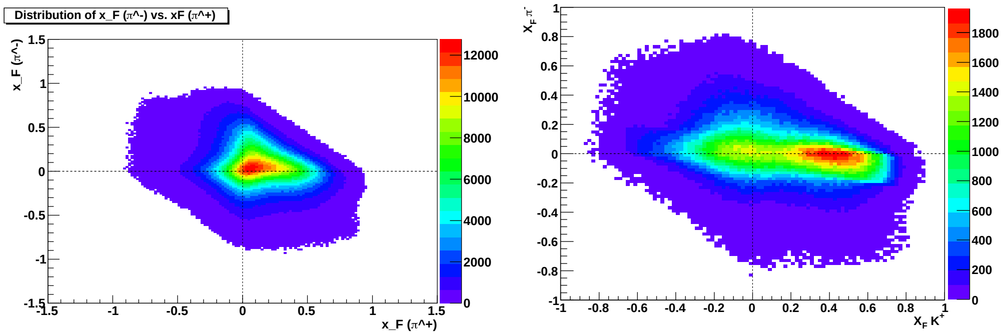

FIG. 14. Distribution over x_F for $\pi^+\pi^-$ (left) and $K^+\pi^-$ pairs from FASTMC

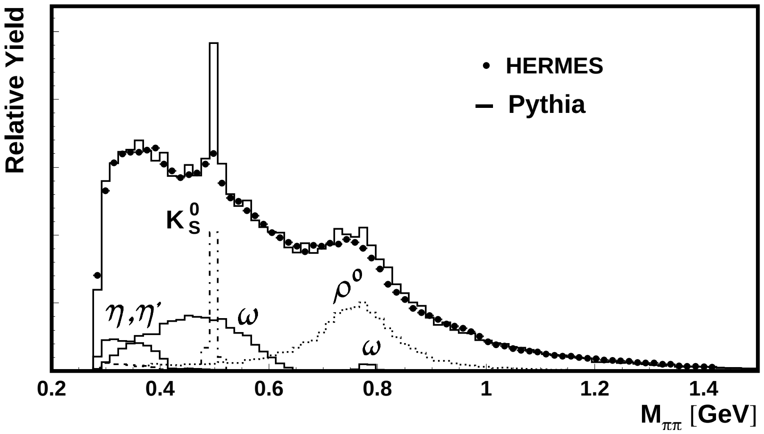

FIG. 15. Typical mass distribution for $\pi^+\pi^-$ dihadrons, including contributions from decays. From [66].

method, including radiative effects, CLAS12 acceptance, and expected beam parameters. We found that the uncertainty on P_T for the proton will be about 3% and on the deuteron about 5%.

1. *Event Selection Criteria*

We focus the analysis on inclusive dihadron production. For each event, we build a list of dihadrons, where each dihadron is a permutation of 2 hadrons from the event, along with the coincident scattered electron. We plan to use particle identification provided by the CLAS12 event builder [97], along with any refinements, to select the dihadron channel of interest as well as the scattered electron. The electron momentum determines the following variables, which are listed here along with criteria for analysis:

- Virtual photon momentum-squared: $Q^2 > 1$ GeV^2, to select the DIS regime
- Invariant mass of proton + photon: $W > 2$ GeV, which is above the resonance region
- Fraction of beam energy carried by photon: $y < 0.8$, since radiative effects are more severe at high y

For the dihadron, denoted h_1h_2, we require

- Fraction of virtual-photon energy carried by the dihadron: $z_{h_1h_2} < 0.95$, to reduce contributions from the exclusive region
- Missing mass: $M_X > 1.5$ GeV, to stay above exclusive events and resonances

- Feynman-x: $x_F > 0$ for each hadron, to enhance the probability that both hadrons are produced in the current fragmentation region

- Hadron momentum: $p_{h_{1,2}} > 1.25$ GeV, to ensure high track reconstruction efficiency

While these cuts are still being refined, their aim is to provide a clean sample of inclusive dihadrons with minimal systematic uncertainties and maximal statistics. These cuts are similar to those used for the CLAS6 analysis on dihadron beam spin asymmetries [118], as well as the recent CLAS12 preliminary results described in section VI B.

Finally, it is worth noting that these cuts can be further tuned for different analyses. For example, while these cuts are well studied for the $\pi\pi$ channel, there may be some alterations or further cuts necessary for πK or KK channels. For the case of DSIDIS, a cut requiring x_F of one hadron to be positive and that of the other hadron to be negative is necessary; however, this may not be sufficient enough to separate the target and current fragmentation regions, requiring further cut refinement.

2. Asymmetry Measurement

There are many techniques to extract the asymmetry from data. Because there are multiple modulations of the dihadron cross section, including partial wave expansions, we employ an unbinned extended maximum likelihood method (MLM).

Let h_b and h_t respectively denote the electron beam helicity and the target helicity. The ratio of the cross section for a particular combination of helicities to the total cross section can be written in terms of the spin asymmetries:

$$\frac{d\sigma_{h_b h_t}}{d\sigma} = \frac{1}{4}\left(1 + h_b A_{LU} + h_t A_{UL} + h_b h_t A_{LL}\right). \tag{69}$$

Without loss of generality, we will proceed with focus on the target spin asymmetry; the same procedure is applicable to beam spin and double spin asymmetries.

Since the focus is on the target spin asymmetry, for brevity we use a single subscript for denoting cross sections corresponding to each target polarization, and sum over the beam polarizations: let $d\sigma_\pm = d\sigma_{+\pm} + d\sigma_{-\pm}$, where $+$ and $-$ respectively denote positive and negative helicity. Equation 69 becomes

$$\frac{d\sigma_\pm}{d\sigma} = \frac{1}{2}\left(1 \pm A_{UL}\right). \tag{70}$$

The asymmetry A_{UL} is written in terms of cross sections for each helicity, which can be converted into yields N, divided by luminosity L and acceptance Ω. This is the experimentally measured asymmetry, which represents a fraction fP of the true asymmetry, where f is the dilution factor and P is the target polarization. In other words:

$$A_{UL} = \frac{d\sigma_+ - d\sigma_-}{d\sigma} \quad \Longrightarrow \quad fPA_{UL} = \frac{N_+/L_+\Omega_+ - N_-/L_-\Omega_-}{N/L\Omega}. \tag{71}$$

We can then define the following probability distributions

$$p_\pm = \frac{N_\pm}{N} = \mu_\pm\left(1 \pm fPA_{LU}\right), \tag{72}$$

where $\mu_\pm = L_\pm\Omega_\pm/2L\Omega$ represents a normalization factor.

Both the numerator and denominator of A_{UL} expand in terms of structure functions, each modulated by functions of ϕ_h, ϕ_R, and θ, and scaled by depolarization factors $k(\varepsilon, y)$. For the unpolarized differential cross section in the denominator, in practice one integrates it to obtain the total cross section; this assumes that the modulations of the unpolarized cross section are linearly independent from a constant, which is not necessarily true, however we will return to this concern later when discussing systematics. The total unpolarized cross section is then the product of the depolarization factor $k_{UU}^{\text{const}} = A(y)$ (see Appendix A) and structure function F_{UU}^{const}, which is $F_{UU,T}$ from equation 5.

Expanding the numerator in terms of modulations $\psi_i(\phi_h, \phi_R, \theta)$, we have

$$A_{UL} = \sum_i \frac{k_{UL}^{\psi_i} F_{UL}^{\psi_i}}{k_{UU}^{\text{const}} F_{UU}^{\text{const}}} \psi_i = \sum_i A_{UL}^{\psi_i} \psi_i, \tag{73}$$

where we have defined

$$A_{UL}^{\psi_i} = K_{UL}^{\psi_i} \frac{F_{UL}^{\psi_i}}{F_{UU}}, \tag{74}$$

with $K_{UL}^{\psi_i} = k_{UL}^{\psi_i}/k_{UU}^{\text{const}}$, the ratio of depolarization factors. $A_{UL}^{\psi_i}$ is the amplitude of the ψ_i modulation of A_{UL}, and it is proportional to a ratio of structure functions.

To isolate the ψ_i modulation amplitude, one can take the ψ_i moment of the numerator and all terms will vanish except for $A_{UL}^{\psi_i}$. In practice however, the modulations ψ_i may not be completely linearly independent; it is therefore more appropriate to implement a simultaneous determination of several modulation amplitudes. We have chosen to perform the simultaneous determination using an unbinned exteneded MLM fit, based on the probability distributions

$$p_\pm = \frac{N_\pm}{N} = \mu_\pm \left(1 \pm fP \sum_i A_{UL}^{\psi_i} \psi_i \right). \tag{75}$$

From here, we can proceed with an extended unbinned MLM fit, which is a standard procedure (see [119], for example). These two probability distributions, one for each target helicity state, are used simultaneously to build an extended likelihood function, which depends on the asymmetry amplitudes and kinematics (independent variables), as well as the normalization. The set of asymmetry amplitudes which maximizes the likelihood function is the result of the fit. In practice, this is a minimization problem since it is computationally favorable to minimize the negative logarithm of the likelihood.

The data over which the likelihood is minimized consist of the yields for each target helicity state. This is a discrete dataset, and therefore must be binned discretely in the full phase space; however, in the *unbinned* limit, the bins are taken to be small enough such that only 0 or 1 event is present in each bin. Finally, the independent normalizations of the two probability densities are allowed to float, which can compensate for any difference in the luminosities from the two target helicities; for this reason, the likelihood fit is called *extended.*

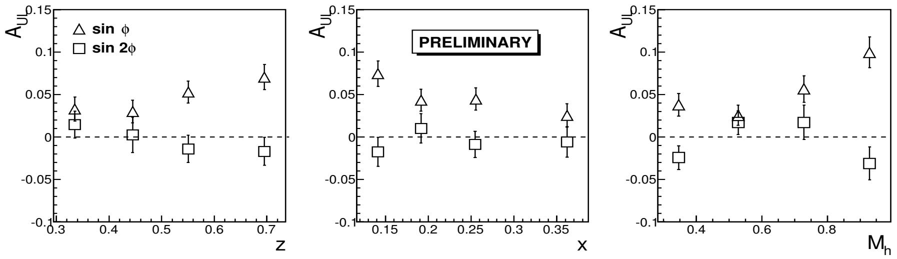

FIG. 16. CLAS6 preliminary target spin asymmetries [3].

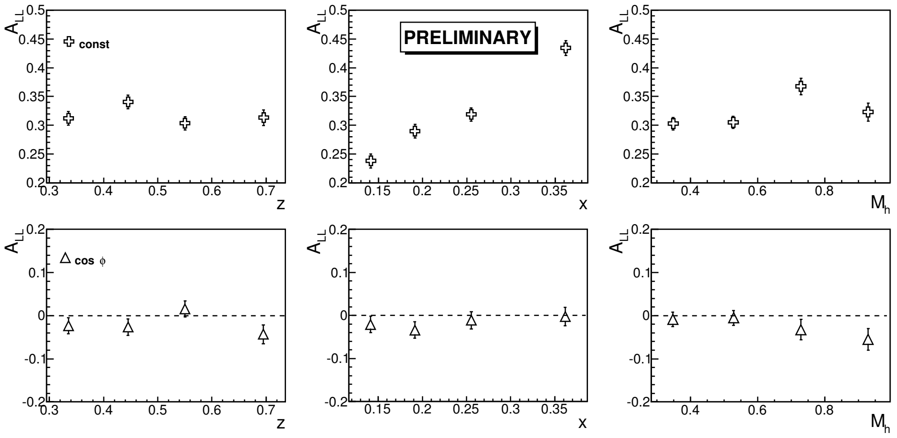

FIG. 17. CLAS6 preliminary double spin asymmetries [3].

VI. Expected results

Before discussing the expected results and projections, it is useful to review the current data on SIDIS dihadron spin asymmetries.

A. Existing data on target spin and double spin asymmetries

Preliminary data from CLAS [3] at 6 GeV indicate large azimuthal $\sin\phi_R$ moments both for unpolarized and polarized targets, that is, in both the beam-spin and the target-spin asymmetries. The target spin asymmetry shown in figure 16 (open-triangles) is sensitive to the collinear twist-3 PDF $h_L(x)$. An additional moment, $\sin(2\phi_R)$, is included in the figure and is consistent with zero; this is a modulation of a twist-2 structure function, which includes a convolution of the wormgear distribution $h_{1L}^{\perp}$ and the IFF $H_{1,TT}^{\sphericalangle}$. Figure 17 shows the double spin asymmetries, where the constant modulation is senstive to $g_1 D_1$ and the $\cos\phi_R$ modulation is sensitive to $g_1\widetilde{D}$, where $\widetilde{D}$ is a twist-3 DiFF; these results indicate that $\widetilde{D}$ is at least an order of magnitude smaller than D_1.

COMPASS also measured various modulations of the target spin and double spin asymmetries in dihadron production from inelastic scattering of muons on a polarized solid ammonia target [4]; this measurement was at a higher energy than at CLAS12, and is sensitive to lower x. Figure 18 shows the average asymmetry amplitudes for a variety of modulations. The $\sin(\phi_h - \phi_R)$ amplitude of the target spin asymmetry, sensitive to the helicity distribution convolved with $G_1^{\perp}$, is consistent with zero even when binned in M_h, although with these uncertainties it is not inconsistent with the spectator model prediction from [88] shown in figure 9. The amplitude $A_{UL}^{\sin\phi_R}$ shows a slight rise as a function of x and of z, up to about 1%; this is at a lower x range than the CLAS6 measurement in figure 16. The other target spin asymmetries correspond to structure functions which involve the wormgear distribution, or higher order partial waves, and are all consistent with or close to zero, as are the double spin asymmetries.

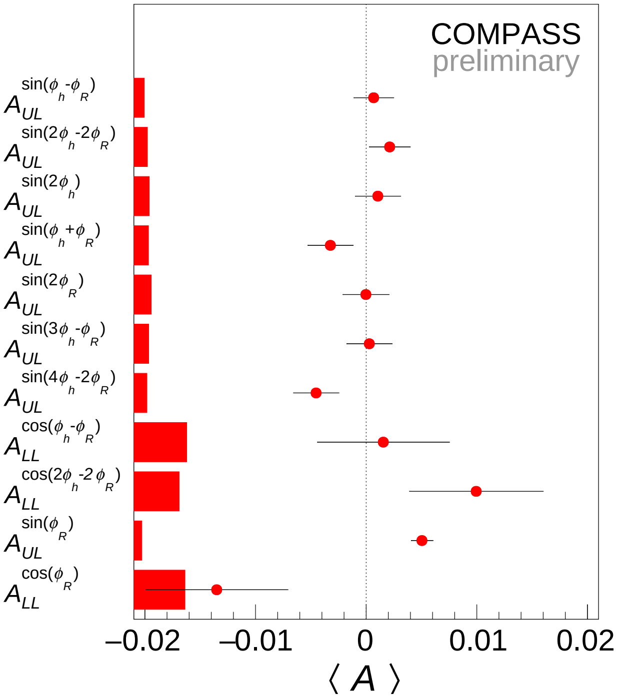

FIG. 18. COMPASS preliminary target spin and double spin asymmetries [4].

HERMES measured transverse target spin asymmetries [66], sensitive to the transversity $h_1(x)$ and the IFF $H_1^{\sphericalangle}$. These measurements, in conjunction with those by Belle on the IFF [62], allowed the extraction of the transversity distribution from SIDIS data [120–122]. Significant asymmetries were observed, and a future program with a transversely polarized target at CLAS12 as well as the EIC can help improve and extend these measurements.

B. Preliminary CLAS12 dihadron beam spin asymmetries

CLAS12 recently released a preliminary measurement of the dihadron beam spin asymmetries, shown in figure 19 [123, 124]. The blue triangles show the $\sin\phi_R$ amplitude which is sensitive to the collinear twist-3 PDF $e(x)$ and shows a rise in M_h to about 4%. The $\sin(\phi_h - \phi_R)$ modulation is sensitive to the helicity DiFF $G_1^{\perp}$, convolved with the unpolarized PDF $f_1(x)$, and exhibits a clear sign change near the ρ-meson mass, somewhat similar to the spectator model from figure 9. The spectator model prediction [88] was for the target spin asymmetry, which involves the helicity distribution instead of $f_1(x)$; since $g(x) < f_1(x)$, it is natural to assume their prediction for the beam spin asymmetry is larger in magnitude, and possibly consistent with these preliminary results. Finally, the $\sin\phi_h$ modulation is included as well, because it turns out that all three amplitudes are linearly dependent and must be fit altogether simultaneously.

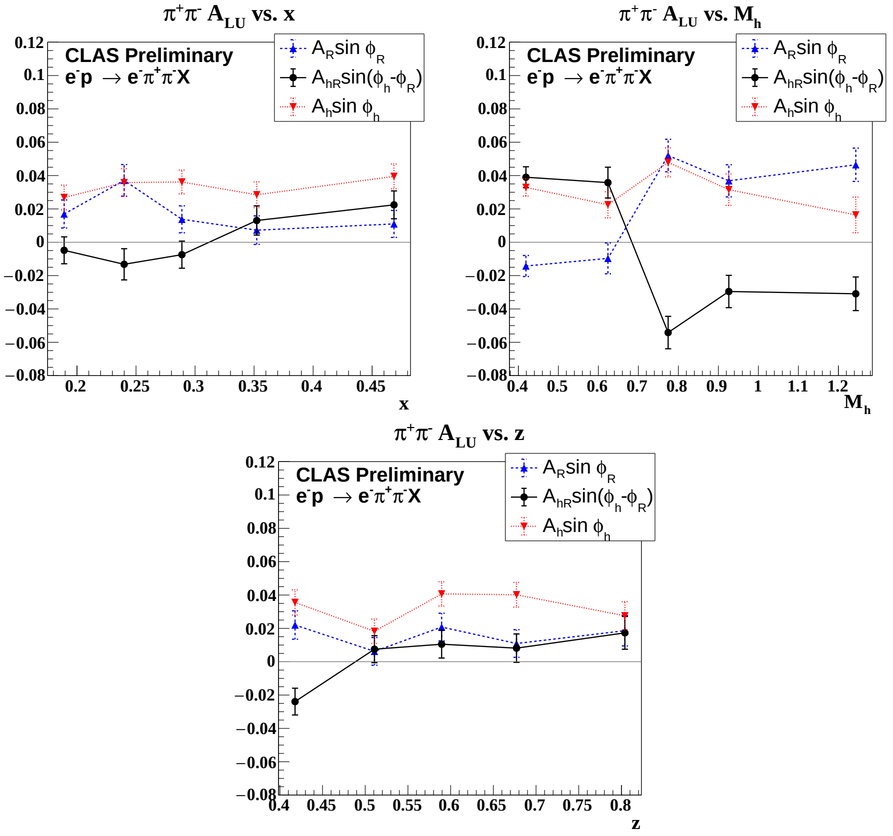

FIG. 19. CLAS12 preliminary results for the beam spin asymmetry [123].

Asymmetry	**Modulation**	**Physics Goal**	**Depolarization Ratio** $K(\varepsilon, y)$	$\langle K(\varepsilon, y)\rangle$
A_{LU}	$\sin(\phi_R)$	$e(x)$	W/A	0.7
	$\sin(\phi_h - \phi_R)$	$G_1^{\perp}$	C/A	0.8
A_{UL}	$\sin(\phi_R)$	$h_L(x)$	V/A	1.3
	$\sin(\phi_h - \phi_R)$	$G_1^{\perp}$	A/A	1
	$\sin(\phi_h + \phi_R)$	$h_{1L}^{\perp}$	B/A	0.6
A_{LL}	$\cos(m\phi_h - m\phi_R)$	$D_1^{\lvert\ell,m\rangle}$	C/A	0.8
	$\cos(\phi_h + \phi_R)$	$\widetilde{D}$	W/A	0.7

TABLE IV. Table of beam spin, target spin, and double spin asymmetries, and corresponding physics goals.

Target	**Dilution** f	**Polarization** P
NH_3	0.2	0.85
ND_3	0.285	0.35
^{3}He	0.27	0.5

TABLE V. Targets along with estimated averages of dilution and polarization.

C. Statistical projections for this proposal

Table IV shows a summary of beam spin, target spin, and double spin asymmetries, along with the primary physics goal, which is a PDF or a DiFF. Shown additionally are the corresponding kinematic depolarization ratios $K(y, \varepsilon)$, which depend on y and ε through equation 3 (see appendix A for definitions), along with their average values based on present CLAS12 data, taken by Run Group A. In the following statistical projections of target spin and double spin asymmetries, we base our predicted statistical uncertainty on the assumption of running on NH_3 and ND_3 targets [125] with 50% efficiency. Note that the shorter data-taking period allocated for the ND_3 target, as compared to that for the NH_3 target, will result in a lower statistical precision for the former measurement, especially at large P_T, because of the lower polarization of ND_3 relative to NH_3. We also include projections for a ^{3}He target, which is a part of another proposal submitted to PAC48 in parallel with this one.

The presented estimated statistical projections are based on effectively running 60, 90, and 120 days, assuming 50% efficiency of running. In principle one could use the fast Monte Carlo to extrapolate asymmetry projections (see appendix C), however given that we have plenty of data from Run Group A, it is simpler and more accurate to extrapolate dihadron yields from the data rate. By counting the number of dihadrons which pass all event selection criteria and a selection of Run Group A data with minimal downtime, we estimate a rate of 5.1 Hz for dihadron acquisition.

In addition to the extrapolated dihadron yield, the polarization and dilution factors are also needed. Table V shows the targets along with mean dilution and polarization factors. Dilution factors for each target, estimated with the Monte Carlo, are shown in figures 20-22, as a function of the relevant kinematic variables. While there is some mild kinematic dependence, we have elected to use the average values of the dilution factors in table V for the statistical projections shown below. Lastly, for projections of the double spin asymmetries, a beam polarization of 0.8 is assumed.

Projections of asymmetries from the ^{3}He target [106], for another experimental proposal also submitted to PAC48, are included as well. Since the goals of measuring dihadrons from the ND_3 target match those from the ^{3}He target, we include additional statistical projections for ^{3}He here for convenient comparison.

In order to estimate the magnitudes of the expected target spin asymmetries, we make use of the CLAS12 preliminary results on the beam spin asymmetries from a proton (p) target, denoted A_{LU}^{p}, and mean kinematic depolarization factors from the data. Note that while it is possible to measure a beam spin asymmetry in parallel with the proposed measurements, it is not the priority. Nonetheless, it may be interesting to at least take a preliminary look at the beam spin asymmetry for the different targets.

First we discuss $A_{UL}^{\sin\phi_R}$, which is sensitive to $h_L(x)$. We first assume that for the unpolarized PDFs, $f^d(x) = 0.4 f^u(x)$. Since some models claim $h_L^u(x)$ to be a bit larger than $e^u(x)$, whereas others claim the opposite, we make the assumption that $h_L^u(x) \approx e^u(x)$. We also make the assumption that $e^d(x)$ can range between 0 and $e^u(x)$, which is motivated by the existing models. The remaining freedom is in the ratio

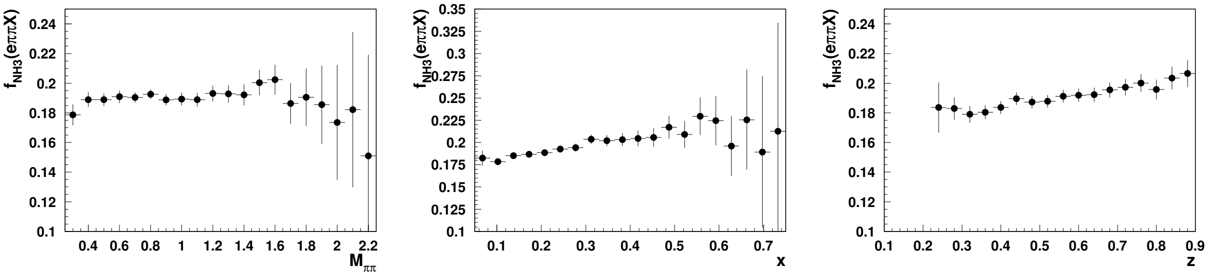

FIG. 20. NH_3 dilution factors versus M_h, x, and z. Only statistical errors shown.

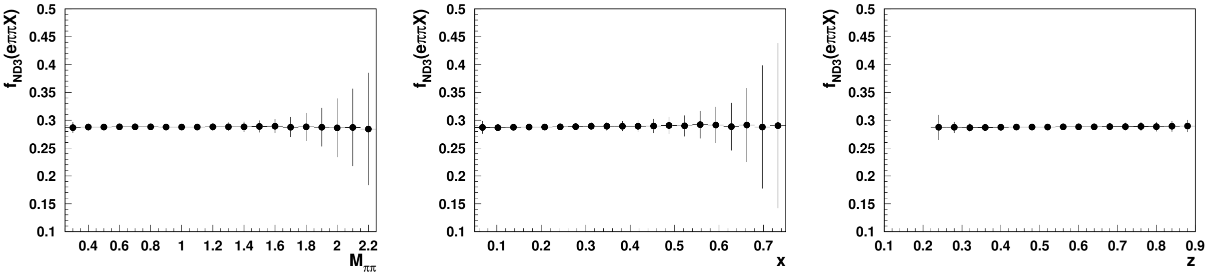

FIG. 21. ND_3 dilution factors versus M_h, x, and z. Only statistical errors shown.

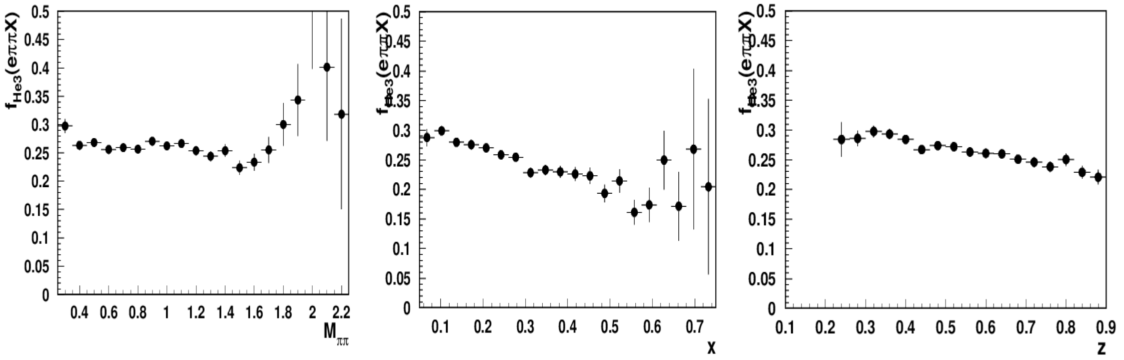

FIG. 22. ^{3}He dilution factors versus M_h, x, and z. Only statistical errors shown.

$R = h_L^d(x)/h_L^u(x)$. Models suggest that R is likely small, and the asymmetries with the smallest magnitudes occur when $|R| < 0.25$, so we will consider this range for our projections. For a proton target, the value of A_{UL}^p is approximately twice the value of A_{LU}^p, for all values of R in the range. For neutrons (n), however, A_{UL}^n is zero for $R = 0.25$, approximately equal to A_{LU}^p for $R = 0$, and approximately twice A_{LU}^p for $R = -0.25$; if $R > 0.25$, then A_{UL}^n will have the opposite sign as A_{LU}^p. We therefore have chosen to plot the projections along a polynomial curve which fits the CLAS12 preliminary data on $k \cdot A_{LU}^p$, where $k = 2$ for the A_{UL}^p projection and $k = 1$ for A_{UL}^n. Figure 23 shows the resulting projections.

For the other primary target spin asymmetry modulation, $A_{UL}^{\sin(\phi_h - \phi_R)}$, the ratio of $A_{UL}^{p,n}$ to A_{LU}^p depends on the ratio of the helicity PDF to the unpolarized PDF. We find that, for approximate values of these PDFs taken at $x \sim 0.3$, $A_{UL}^p \approx 0.4 A_{LU}^p$ and $A_{UL}^n \approx -0.05 A_{LU}^p$. The smaller target spin asymmetry, relative to the beam spin asymmetry, is compatible with the recent spectator model predictions [88], so we have therefore decided to draw the prediction for A_{UL}^p along a curve which approximates the spectator model prediction. On the other hand, the prediction for A_{UL}^n will likely be too small to be statistically discernible from zero, so its projection is omitted.

Fig 24 shows the projection for $A_{UL}^{\sin(\phi_h - \phi_R)}$ with a proton target. The data points are positioned along a curve which approximately follows the spectator model prediction [88][7]. The run time with 60 days is shown in the left panel, but with an expected maximum amplitude of 1%, the signal will not be sufficiently significant; the right panel shows a comparison for 120 days of running with no downtime.

Figure 25 shows the projected statistical uncertainties for the $\cos\phi_R$ modulation of A_{LL}, which is sensitive to the twist-3 TMD PDF e_L convolved with the IFF $H_1^{\sphericalangle}$, summed with the helicity $g_1(x)$ convolved with the twist-3 DiFF $\widetilde{D}$. Since e_L is not collinear, it will vanish under an integral over the quark transverse momentum, thus a measurement of this asymmetry can constrain the twist-3 DiFF $\widetilde{D}$. Measurements of the collinear twist-3 PDFs $e(x)$ and $h_L(x)$ include an additional term involving the twist-3 DiFF $\widetilde{G}$, which is thought to be smaller than $\widetilde{D}$. Thus a constraint on $\widetilde{D}$ can in turn help further constrain $e(x)$ and $h_L(x)$. COMPASS and CLAS6 measurements of this asymmetry were consistent with zero [3, 4], so the projected points are also set to zero; no model is assumed and figure 25 shows only statistical projections.

The numerical values for these projections are given in tables VI-XII. The first and second columns give the bins in which the asymmetries are shown, written as the bin range and mean. In all projections, the bin boundaries are chosen as quantiles. The third column is the value of the asymmetry (only reported in tables VI-IX), and the remaining columns gives its projected statistical uncertainty, assuming 60, 90, and 120 days, with 50% efficiency of running.

Although we have not prepared projections for the DSIDIS process, we again remark that careful studies of the separation of the current and target fragmentation regions are needed. As a first step toward this separation, we can compare the ratio of the number of dihadrons where one hadron has $x_F < 0$ with the other having $x_F > 0$, to the number of current fragmentation region dihadrons, where both hadrons have $x_F > 0$. In Run Group A data the ratio is approximately 15% or 5% for $\pi^+\pi^-$ dihadrons, and it depends on which hadron is associated with which x_F cut. Thus the estimated statistical uncertainty of DSIDIS asymmetries may be a factor of 2–4 times larger than those presented in figures 23-25. If the asymmetries are not large, then at least a measurement of DSIDIS asymmetries could provide upper bounds and still constrain the fracture functions.

---

[7] Although these predictions are for COMPASS and EIC energies, the dependence of the model on $\sqrt{s}$ appears to be negligible.

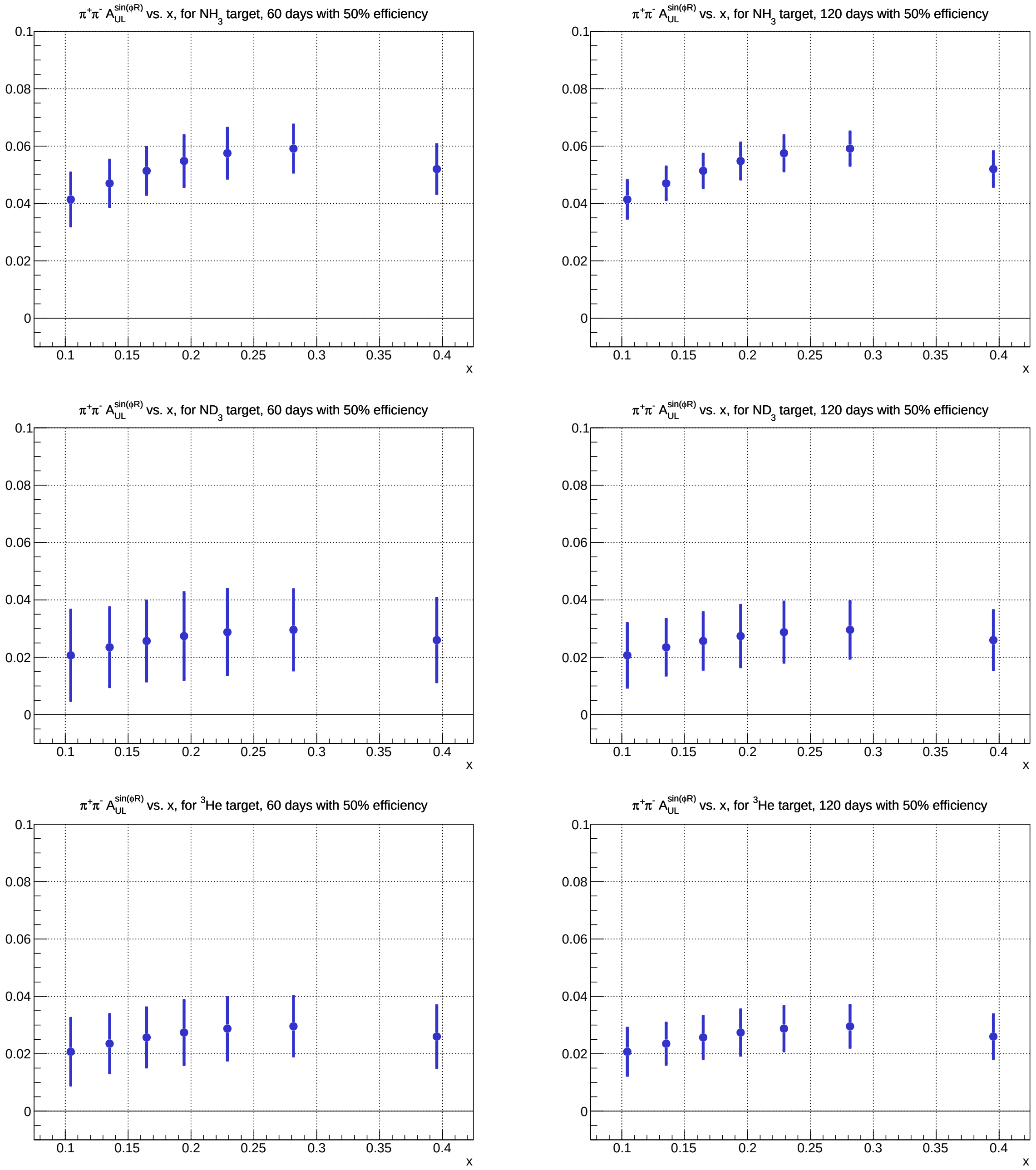

FIG. 23. Projection of the $\sin\phi_R$ modulation of A_{UL}, versus x, for 60 days (left column) and for 120 days (right column). Three targets are shown: NH_3 (top row), ND_3 (middle row), and ^{3}He (bottom row). See text for details.

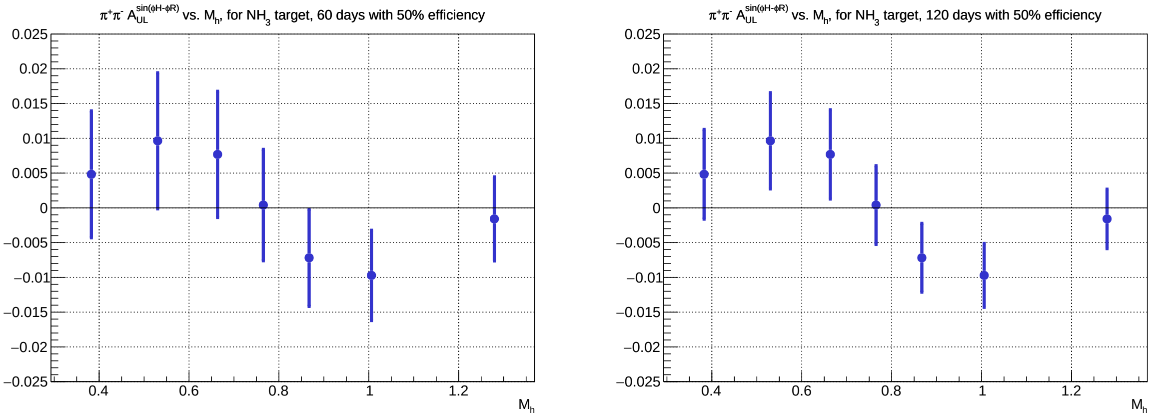

FIG. 24. Projection of the $\sin(\phi_h - \phi_R)$ modulation of A_{UL} with the NH_3 target, versus M_h, for 60 days (left) and for 120 days (right). See text for details.

x range	$\langle x \rangle$	A_{UL}	60 days σ	90 days σ	120 days σ
[0.00, 0.12)	0.1	0.041	0.0092	0.0075	0.0065
[0.12, 0.15)	0.14	0.047	0.0081	0.0066	0.0057
[0.15, 0.18)	0.16	0.051	0.0082	0.0067	0.0058
[0.18, 0.21)	0.19	0.055	0.0089	0.0072	0.0063
[0.21, 0.25)	0.23	0.058	0.0087	0.0071	0.0062
[0.25, 0.32)	0.28	0.059	0.0082	0.0067	0.0058
[0.32, 1.00)	0.4	0.052	0.0085	0.007	0.006

TABLE VI. Data table for projection of $A_{UL}^{\sin \phi_R}$ in bins of x, for the NH_3 target. See figure 23, top row.

x range	$\langle x \rangle$	A_{UL}	60 days σ	90 days σ	120 days σ
[0.00, 0.12)	0.1	0.021	0.016	0.013	0.011
[0.12, 0.15)	0.14	0.024	0.014	0.011	0.0097
[0.15, 0.18)	0.16	0.026	0.014	0.011	0.0099
[0.18, 0.21)	0.19	0.027	0.015	0.012	0.011
[0.21, 0.25)	0.23	0.029	0.015	0.012	0.01
[0.25, 0.32)	0.28	0.03	0.014	0.011	0.0099
[0.32, 1.00)	0.4	0.026	0.015	0.012	0.01

TABLE VII. Data table for projection of $A_{UL}^{\sin \phi_R}$ in bins of x, for the ND_3 target. See figure 23, middle row.

x range	$\langle x \rangle$	A_{UL}	60 days σ	90 days σ	120 days σ
[0.00, 0.12)	0.1	0.021	0.012	0.0095	0.0082
[0.12, 0.15)	0.14	0.024	0.01	0.0083	0.0072
[0.15, 0.18)	0.16	0.026	0.01	0.0084	0.0073
[0.18, 0.21)	0.19	0.027	0.011	0.0091	0.0079
[0.21, 0.25)	0.23	0.029	0.011	0.0089	0.0077
[0.25, 0.32)	0.28	0.03	0.01	0.0084	0.0073
[0.32, 1.00)	0.4	0.026	0.011	0.0088	0.0076

TABLE VIII. Data table for projection of $A_{UL}^{\sin \phi_R}$ in bins of x, for the ^3He target. See figure 23, bottom row.

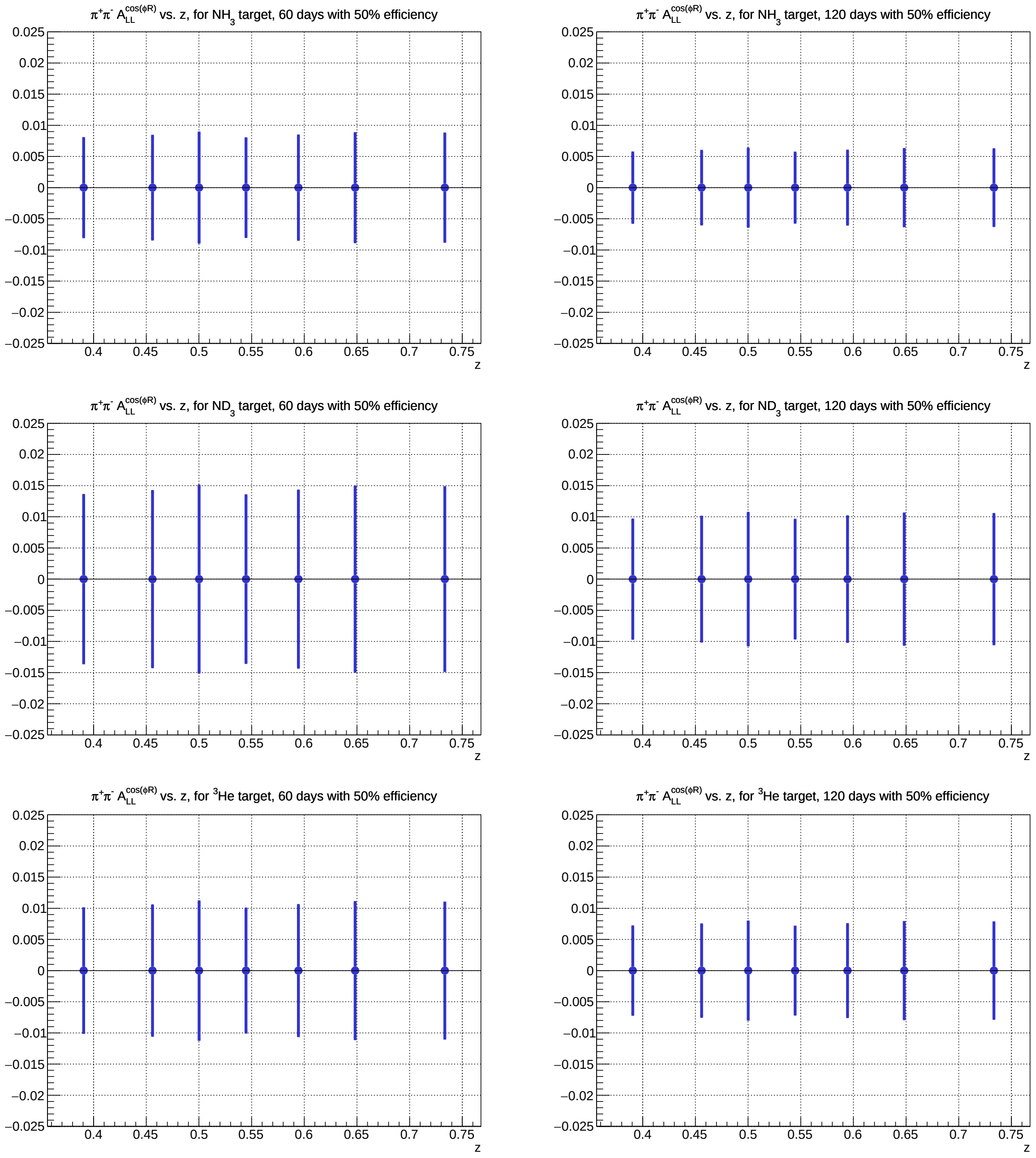

FIG. 25. Projected statistical uncertainties of the $\cos\phi_R$ modulation of A_{LL}, versus z, for 60 days (left column) and for 120 days (right column). Three targets are shown: NH_3 (top row), ND_3 (middle row), and ^{3}He (bottom row). See text for details.

M_h range	$\langle M_h \rangle$	A_{UL}	60 days σ	90 days σ	120 days σ
[0.00, 0.46)	0.38	0.0048	0.0091	0.0074	0.0064
[0.46, 0.60)	0.53	0.0096	0.0098	0.008	0.0069
[0.60, 0.72)	0.66	0.0077	0.0091	0.0074	0.0064
[0.72, 0.81)	0.77	0.0004	0.008	0.0065	0.0057
[0.81, 0.93)	0.87	-0.0072	0.007	0.0057	0.0049
[0.93, 1.10)	1	-0.0097	0.0065	0.0053	0.0046
[1.10, 3.00)	1.3	-0.0016	0.006	0.0049	0.0043

TABLE IX. Data table for projection of $A_{UL}^{\sin(\phi_h-\phi_R)}$ in bins of M_h, for the NH_3 target. See figure 24.

z range	$\langle z \rangle$	60 days σ	90 days σ	120 days σ
[0.00, 0.43)	0.39	0.0079	0.0064	0.0056
[0.43, 0.48)	0.46	0.0083	0.0067	0.0058
[0.48, 0.52)	0.5	0.0088	0.0072	0.0062
[0.52, 0.57)	0.54	0.0079	0.0064	0.0056
[0.57, 0.62)	0.59	0.0083	0.0068	0.0059
[0.62, 0.68)	0.65	0.0087	0.0071	0.0061
[0.68, 1.00)	0.73	0.0086	0.007	0.0061

TABLE X. Data table for projected statistical uncertainties of $A_{LL}^{\cos\phi_R}$ in bins of z, for the NH_3 target. See figure 25, top row.

z range	$\langle z \rangle$	60 days σ	90 days σ	120 days σ
[0.00, 0.43)	0.39	0.013	0.011	0.0095
[0.43, 0.48)	0.46	0.014	0.011	0.01
[0.48, 0.52)	0.5	0.015	0.012	0.011
[0.52, 0.57)	0.54	0.013	0.011	0.0095
[0.57, 0.62)	0.59	0.014	0.012	0.01
[0.62, 0.68)	0.65	0.015	0.012	0.01
[0.68, 1.00)	0.73	0.015	0.012	0.01

TABLE XI. Data table for projected statistical uncertainties of $A_{LL}^{\cos\phi_R}$ in bins of z, for the ND_3 target. See figure 25, middle row.

z range	$\langle z \rangle$	60 days σ	90 days σ	120 days σ
[0.00, 0.43)	0.39	0.0099	0.0081	0.007
[0.43, 0.48)	0.46	0.01	0.0085	0.0074
[0.48, 0.52)	0.5	0.011	0.009	0.0078
[0.52, 0.57)	0.54	0.0099	0.0081	0.007
[0.57, 0.62)	0.59	0.01	0.0085	0.0074
[0.62, 0.68)	0.65	0.011	0.0089	0.0077
[0.68, 1.00)	0.73	0.011	0.0089	0.0077

TABLE XII. Data table for projected statistical uncertainties of $A_{LL}^{\cos\phi_R}$ in bins of z, for the ^{3}He target. See figure 25, bottom row.

Systematic Uncertainty Contributor	A_{LU}	A_{UL}	A_{LL}
beam polarization	3%	-	3%
target polarization	-	3%	3%
dilution factor	-	4%	4%
transverse (to γ^*) spin effects	-	3%	3%
radiative corrections	3%	3%	3%
acceptance	20%	20%	20%
baryonic resonances	14%	14%	14%
higher order partial waves of σ_{UU}	10%	10%	10%

TABLE XIII. Uncertainties for asymmetry measurements.

D. Systematic Uncertainty

The proposed spin asymmetry measurements are rather insensitive to uncertainties in acceptances and charge normalization, since those are independent of helicity and largely cancel in a ratio of cross sections. There are systematic uncertainty contributions that do impact the asymmetry magnitude, however, as listed in Table XIII. The numbers listed are rough estimates, based on past measurements and experience such as HERMES [66], and on present experience with CLAS6 [118] and CLAS12 beam spin asymmetries [123, 124]. These estimates only serve as an illustration of the possible magnitude of the systematic uncertainties; for a more accurate determination of a systematic uncertainty, careful analysis of the dataset is needed.

The uncertainty on the target polarization contributes to a systematic uncertainty on the scale of target spin asymmetries, and double spin asymmetries receive an additional systematic uncertainty contribution from the beam polarization uncertainty. The uncertainty on the dilution factor also contributes, along with the ratio of the longitudinal to transverse photo-absorption cross section. The other uncertainties require more thorough study to understand, and many require the data to be acquired.

Uncertainty from radiative corrections originate from correcting for QED effects. The acceptance contribution can be obtained by comparisons of data and Monte Carlo. Some dihadrons can come from baryonic resonances, which if one chooses to subtract them out of the asymmetry as a background contribution, can result in an asymmetry with a different scale. Lastly, dihadrons from vector meson decays can in-turn contribute to higher order partial waves of the unpolarized dihadron fragmentation function.

With these estimates, the quadrature sum gives a total systematic uncertainty on the asymmetry scale of about 27% (if we exclude the contribution from baryonic resonances, the total is 23%). For an asymmetry of 0.02, the systematic uncertainty is ±0.005; the binning used in the above projections gives statistical uncertainties of $\sim 1\%$, which is still larger than the systematic uncertainty, but does present itself as approaching a limit to how finely the measurement can be binned, either one-dimensionally or multi-dimensionally.

VII. Summary and Request

Detailed measurements of target spin and double spin asymmetries as a function of relevant kinematical variables in different bins in x, z, Q^2, M_h combined with measurements of single-pion and single-kaon measurements [8, 10] will allow to study the underlying distributions and fragmentation processes. The use of different polarized targets, such as NH_3 and ND_3, will provide access to flavor dependence, while kaon identification provided by the RICH will allow detection of pion-kaon and kaon-kaon pairs, allowing for studies of the effect of strange and non-strange sea on the flavor and spin structure of the nucleon.

In recent years, significant experimental and theoretical efforts have been made to understand QCD beyond twist-2. Twist-3 functions, describing multiparton correlations corresponding to the interference of higher Fock components in the hadron wave functions, offer fascinating insights into the nucleon structure. In particular, they describe effects of the transverse color force on quarks, along with correlations between the color magnetic field and the spin of the nucleon [13, 14].

The main goal of the proposal is to extract information on the twist-3 collinear PDFs $e(x)$ and $h_L(x)$, using the recent progress in understanding of dihadron fragmentation functions (DiFFs) and their extraction from e^+e^- data. The formalism of DiFFs is based on collinear factorization with well defined evolution equations. The plan is to gather a data set on hadron pairs produced from SIDIS in the region $0.1 \leq x \leq 0.8$, $0.5 \leq M_h \leq 1.2$, and $0.2 \leq z \leq 0.8$. Global analysis of the data will provide fits to higher twist distribution functions $e(x)$ and $h_L(x)$. Furthermore, double spin asymmetries can help establish limits on the twist-3 dihadron fragmentation functions, which in turn help with the extractions of $e(x)$ and $h_L(x)$.

The measurements outlined in this proposal include subleading twist asymmetries, which offer valuable insights toward understanding why subleading twist effects appear to be larger than leading twist effects ($A_{UU}^{\cos\phi}$ was larger than $A_{UU}^{\cos 2\phi}$ [126], $A_{UL}^{\sin\phi}$ was larger than $A_{UL}^{\sin 2\phi}$ [15]). Precise data on the production of dihadrons would have an important impact, and motivate further theoretical studies. Ultimately, through a global study of all of these observables, one could simultaneously obtain better knowledge of twist-3 collinear functions and twist-2 TMDs, and at the same time test the validity of the formalism.

These data will also help constrain the helicity-dependent dihadron fragmentation function $G_1^\perp$, along with its partial waves. $G_1^\perp$ is sensitive to spin-momentum correlations in hadronization, and may require the interference with a transversely polarized dihadron. Preliminary measurements of beam spin asymmetries at CLAS12 provide the first experimental evidence of a sizeable $G_1^\perp$, and additionally, indication of a possible sign change of $G_1^\perp$ above and below the ρ-resonance mass. The proposed target spin asymmetry measurements will serve to complement the beam spin asymmetry, helping constrain $G_1^\perp$. Furthermore, the selection of different partial waves can also help pin down production mechanisms of dihadrons with a particular angular momentum, such as those from ρ-meson decays. In particular, partial waves of the unpolarized dihadron fragmentation function are also accessible, via double spin asymmetry measurements.

Another interesting topic of exploration is dihadrons with one hadron produced in the current fragmentation region and the other in the target fragmentation region. This process is known as Double SIDIS [93], and is sensitive to the fracture functions, which describe the probability of the production of a hadron in the target fragmentation region, on the condition that a quark in the target was struck and later fragments into additional hadrons. The large acceptance at CLAS allows for the unique opportunity for this measurement.

The proposed set of measurements with longitudinally polarized proton and deuteron targets will yield a comprehensive set of azimuthal moments in spin-dependent and independent SIDIS, providing access to corresponding distribution and fragmentation functions in a wide range of x, Q^2, z, and M_h. Our data, combined with the data from HERMES, COMPASS, and Belle, will provide independent (complementary to e^+/e^-) measurements of polarized pion and kaon DiFFs and will allow a study of leading twist distributions complementary to single hadron SIDIS analyses.

To achieve this goal we request to run as a Run Group C addition, with an 11 GeV highly polarized electron beam in Hall B with a luminosity of $10^{35}\text{cm}^{-2}\text{sec}^{-1}$. The PAC has approved 120 days for NH_3 and 60 days for ND_3 (as well as 5 days for ^{15}N). The proposed ^3He target, also submitted to PAC48, offers an additional target option for measurements with polarized neutrons, which could be combined with the proposed measurements with the ND_3 target, ultimately achieving similar statistical precision of asymmetries from both polarized protons and polarized neutrons. We conclude by noting that while the measurements in this proposal require a substantial commitment of beam time, we will simultaneously take data with already approved Run Group C experiments [7–10].

Appendices

A. Depolarization Factors

The depolarization factors from Eq.2 can be written as

$$\begin{aligned}
\frac{y^2}{2\,(1-\varepsilon)} &= \frac{1}{1+\gamma^2}\left(1-y+\tfrac{1}{2}y^2+\tfrac{1}{4}\gamma^2y^2\right) &&\approx \left(1-y+\tfrac{1}{2}y^2\right)\equiv A(y), && (76)\\
\frac{y^2}{2\,(1-\varepsilon)}\,\varepsilon &= \frac{1}{1+\gamma^2}\left(1-y-\tfrac{1}{4}\gamma^2y^2\right) &&\approx (1-y)\equiv B(y), && (77)\\
\frac{y^2}{2\,(1-\varepsilon)}\,\sqrt{2\,\varepsilon(1+\varepsilon)} &= \frac{1}{1+\gamma^2}\,(2-y)\,\sqrt{1-y-\tfrac{1}{4}\gamma^2y^2} &&\approx (2-y)\,\sqrt{1-y}\equiv V(y), && (78)\\
\frac{y^2}{2\,(1-\varepsilon)}\,\sqrt{2\,\varepsilon(1-\varepsilon)} &= \frac{1}{\sqrt{1+\gamma^2}}\,y\,\sqrt{1-y-\tfrac{1}{4}\gamma^2y^2} &&\approx y\,\sqrt{1-y}\equiv W(y), && (79)\\
\frac{y^2}{2\,(1-\varepsilon)}\,\sqrt{1-\varepsilon^2} &= \frac{1}{\sqrt{1+\gamma^2}}\,y\left(1-\tfrac{1}{2}y\right) &&\approx y\left(1-\tfrac{1}{2}y\right)\equiv C(y). && (80)
\end{aligned}$$

B. Convolutions

For an arbitrary function $w(\mathbf{k},\mathbf{p})$ we introduce the notation

$$C[\hat{M}\cdot D\,w]=\sum_a e_a^2\int d^2\mathbf{k}\,d^2\mathbf{p}\,\delta^{(2)}(z\mathbf{k}+\mathbf{p}-\mathbf{P}_{T1})\,\hat{M}_a(x,\zeta,\mathbf{k}^2,\mathbf{P}_{T2}^2,\mathbf{k}\cdot\mathbf{P}_{T2})D_a(z,\mathbf{p}^2)\,w, \tag{81}$$

where $\mathbf{k},\mathbf{P}_{T1}$ and $\mathbf{P}_{T2}$ are the two-dimensional transverse momenta of quark, hadrons 1 and 2 with respect to virtual photon momentum and $\mathbf{p}$ is a hadron 1 transverse momentum with respect to fragmenting quark momentum. Then, using the identity for Kronecker delta-function in two-dimensional vectors space

$$\left(\mathbf{P}_{T1}^2\mathbf{P}_{T2}^2-(\mathbf{P}_{T1}\cdot\mathbf{P}_{T2})^2\right)\delta^{ij}=\mathbf{P}_{T2}^2P_{T1}^iP_{T1}^j+\mathbf{P}_{T1}^2P_{T2}^iP_{T2}^j-(\mathbf{P}_{T1}\cdot\mathbf{P}_{T2})\left(P_{T1}^iP_{T2}^j+P_{T1}^jP_{T2}^i\right), \tag{82}$$

we have the following general tensorial decomposition over independent structures:

$$\begin{aligned}
C[\hat{M}\cdot D] &= F_0^{\hat{M}\cdot D}\,,\\
C[\hat{M}\cdot D\,k^i] &= P_{T1}^i\,F_{k1}^{\hat{M}\cdot D}+P_{T2}^i\,F_{k2}^{\hat{M}\cdot D}\,,\\
C[\hat{M}\cdot D\,p^i] &= P_{T1}^i\,F_{p1}^{\hat{M}\cdot D}+P_{T2}^i\,F_{p2}^{\hat{M}\cdot D}\,,\\
C[\hat{M}\cdot D\,k^ik^j] &= P_{T1}^iP_{T1}^j\,F_{kk1}^{\hat{M}\cdot D}+P_{T2}^iP_{T2}^j\,F_{kk2}^{\hat{M}\cdot D}+\delta^{ij}\,F_{kk3}^{\hat{M}\cdot D}\,,\\
C[\hat{M}\cdot D\,k^ip^j] &= P_{T1}^iP_{T1}^j\,F_{kp1}^{\hat{M}\cdot D}+P_{T2}^iP_{T2}^j\,F_{kp2}^{\hat{M}\cdot D}+\left(P_{T1}^iP_{T2}^j-P_{T1}^jP_{T2}^i\right)\,F_{kp3}^{\hat{M}\cdot D}+\delta^{ij}\,F_{kp4}^{\hat{M}\cdot D}\,,\\
C[\hat{M}\cdot D\,k^ik^jp^k] &= P_{T1}^iP_{T1}^jP_{T1}^k\,F_{kkp1}^{\hat{M}\cdot D}+P_{T1}^iP_{T1}^jP_{T2}^k\,F_{kkp2}^{\hat{M}\cdot D}+P_{T2}^iP_{T2}^jP_{T2}^k\,F_{kkp3}^{\hat{M}\cdot D}+P_{T2}^iP_{T2}^jP_{T1}^k\,F_{kkp4}^{\hat{M}\cdot D}\\
&\quad+P_{T1}^k\delta^{ij}\,F_{kkp5}^{\hat{M}\cdot D}+P_{T2}^k\delta^{ij}\,F_{kkp6}^{\hat{M}\cdot D}\,.
\end{aligned} \tag{83}$$

Note, that the functions in the r.h.s. of above equations depend on $x,z,\zeta,\mathbf{P}_{T1}^2,\mathbf{P}_{T2}^2,\mathbf{P}_{T1}\cdot\mathbf{P}_{T2}$.

From Eq.(83), after contracting by appropriate tensorial combinations, constructed from components of $\mathbf{P}_{T1}$ and $\mathbf{P}_{T2}$ and δ^{ij}, we can easily obtain

$$\begin{aligned}
F_{k1}^{\hat{M}\cdot D} &= C\left[\hat{M}\cdot D\frac{(\mathbf{P}_{T1}\cdot\mathbf{P}_{T2})(\mathbf{P}_{T2}\cdot\mathbf{k})-(\mathbf{P}_{T1}\cdot\mathbf{k})\mathbf{P}_{T2}^2}{(\mathbf{P}_{T1}\cdot\mathbf{P}_{T2})^2-\mathbf{P}_{T1}^2\mathbf{P}_{T2}^2}\right],\\
F_{k2}^{\hat{M}\cdot D} &= C\left[\hat{M}\cdot D\frac{(\mathbf{P}_{T1}\cdot\mathbf{k})(\mathbf{P}_{T1}\cdot\mathbf{P}_{T2})-(\mathbf{P}_{T2}\cdot\mathbf{k})\mathbf{P}_{T1}^2}{(\mathbf{P}_{T1}\cdot\mathbf{P}_{T2})^2-\mathbf{P}_{T1}^2\mathbf{P}_{T2}^2}\right].
\end{aligned} \tag{84}$$

$$\begin{aligned}
F_{p1}^{\hat{M}\cdot D} &= C\left[\hat{M}\cdot D\frac{(\mathbf{P}_{T1}\cdot\mathbf{P}_{T2})(\mathbf{P}_{T2}\cdot\mathbf{p})-(\mathbf{P}_{T1}\cdot\mathbf{p})\mathbf{P}_{T2}^2}{(\mathbf{P}_{T1}\cdot\mathbf{P}_{T2})^2-\mathbf{P}_{T1}^2\mathbf{P}_{T2}^2}\right],\\
F_{p2}^{\hat{M}\cdot D} &= C\left[\hat{M}\cdot D\frac{(\mathbf{P}_{T1}\cdot\mathbf{p})(\mathbf{P}_{T1}\cdot\mathbf{P}_{T2})-(\mathbf{P}_{T2}\cdot\mathbf{p})\mathbf{P}_{T1}^2}{(\mathbf{P}_{T1}\cdot\mathbf{P}_{T2})^2-\mathbf{P}_{T1}^2\mathbf{P}_{T2}^2}\right].
\end{aligned}\tag{85}$$

$$\begin{aligned}
F_{kk1}^{\hat{M}\cdot D} &= C\left[\hat{M}\cdot D\,\frac{\left(-2\left(\mathbf{P}_{T1}\cdot\mathbf{k}\right)^2+\mathbf{k}^2\mathbf{P}_{T1}^2\right)\mathbf{P}_{T2}^4+\left(2\left(\mathbf{P}_{T2}\cdot\mathbf{k}\right)^2-\mathbf{k}^2\mathbf{P}_{T2}^2\right)\left(2\left(\mathbf{P}_{T1}\cdot\mathbf{P}_{T2}\right)^2-\mathbf{P}_{T1}^2\mathbf{P}_{T2}^2\right)}{4\left(\mathbf{P}_{T1}\cdot\mathbf{P}_{T2}\right)^2\left(\left(\mathbf{P}_{T1}\cdot\mathbf{P}_{T2}\right)^2-\mathbf{P}_{T1}^2\mathbf{P}_{T2}^2\right)}\right],\\
F_{kk2}^{\hat{M}\cdot D} &= C\left[\hat{M}\cdot D\,\frac{\left(2\left(\mathbf{P}_{T1}\cdot\mathbf{P}_{T2}\right)^2-\mathbf{P}_{T1}^2\mathbf{P}_{T2}^2\right)\left(\mathbf{P}_{T1}\cdot\mathbf{k}\right)^2+\mathbf{P}_{T1}^2\left(\mathbf{P}_{T1}^2\mathbf{P}_{T2}^2-\left(\mathbf{P}_{T1}\cdot\mathbf{P}_{T2}\right)^2\right)\mathbf{k}^2-\left(\mathbf{P}_{T2}\cdot\mathbf{k}\right)^2\mathbf{P}_{T1}^4}{2\left(\mathbf{P}_{T1}\cdot\mathbf{P}_{T2}\right)^2\left(\left(\mathbf{P}_{T1}\cdot\mathbf{P}_{T2}\right)^2-\mathbf{P}_{T1}^2\mathbf{P}_{T2}^2\right)}\right],\\
F_{kk3}^{\hat{M}\cdot D} &= C\left[\hat{M}\cdot D\,\frac{\left(\left(\mathbf{P}_{T1}\cdot\mathbf{P}_{T2}\right)^2+\mathbf{P}_{T1}^2\mathbf{P}_{T2}^2\right)\mathbf{k}^2-\left(\mathbf{P}_{T2}\cdot\mathbf{k}\right)^2\mathbf{P}_{T1}^2-\left(\mathbf{P}_{T1}\cdot\mathbf{k}\right)^2\mathbf{P}_{T2}^2}{2\left(\mathbf{P}_{T1}\cdot\mathbf{P}_{T2}\right)^2}\right].
\end{aligned}\tag{86}$$

$$\begin{aligned}
F_{kp1}^{\hat{M}\cdot D} &= C\Bigg[\hat{M}\cdot D\,\Bigg(\frac{\left(-2(\mathbf{P}_{T1}\cdot\mathbf{k})(\mathbf{P}_{T1}\cdot\mathbf{p})+(\mathbf{k}\cdot\mathbf{p})\mathbf{P}_{T1}^2\right)\mathbf{P}_{T2}^4}{4\left(\mathbf{P}_{T1}\cdot\mathbf{P}_{T2}\right)^2\left(\left(\mathbf{P}_{T1}\cdot\mathbf{P}_{T2}\right)^4-\mathbf{P}_{T1}^2\mathbf{P}_{T2}^2\right)}+\\
&\qquad\frac{\left(2(\mathbf{P}_{T2}\cdot\mathbf{k})(\mathbf{P}_{T2}\cdot\mathbf{p})-(\mathbf{k}\cdot\mathbf{p})\mathbf{P}_{T2}^2\right)\left(2\left(\mathbf{P}_{T1}\cdot\mathbf{P}_{T2}\right)^2-\mathbf{P}_{T1}^2\mathbf{P}_{T2}^2\right)}{4\left(\mathbf{P}_{T1}\cdot\mathbf{P}_{T2}\right)^2\left(\left(\mathbf{P}_{T1}\cdot\mathbf{P}_{T2}\right)^4-\mathbf{P}_{T1}^2\mathbf{P}_{T2}^2\right)}\Bigg)\Bigg],\\
F_{kp2}^{\hat{M}\cdot D} &= C\Bigg[\hat{M}\cdot D\,\Bigg(\frac{\left(\mathbf{P}_{T1}\cdot\mathbf{k}\right)\left(\mathbf{P}_{T1}\cdot\mathbf{p}\right)\left(2\left(\mathbf{P}_{T1}\cdot\mathbf{P}_{T2}\right)^2-\mathbf{P}_{T1}^2\mathbf{P}_{T2}^2\right)}{2\left(\mathbf{P}_{T1}\cdot\mathbf{P}_{T2}\right)^2\left(\left(\mathbf{P}_{T1}\cdot\mathbf{P}_{T2}\right)^2-\mathbf{P}_{T1}^2\mathbf{P}_{T2}^2\right)}-\\
&\qquad\frac{\left(\mathbf{P}_{T2}\cdot\mathbf{k}\right)\left(\mathbf{P}_{T2}\cdot\mathbf{p}\right)\mathbf{P}_{T1}^4+\left(\mathbf{k}\cdot\mathbf{p}\right)\mathbf{P}_{T1}^2\left(\mathbf{P}_{T1}^2\mathbf{P}_{T2}^2-\left(\mathbf{P}_{T1}\cdot\mathbf{P}_{T2}\right)^2\right)}{2\left(\mathbf{P}_{T1}\cdot\mathbf{P}_{T2}\right)^2\left(\left(\mathbf{P}_{T1}\cdot\mathbf{P}_{T2}\right)^2-\mathbf{P}_{T1}^2\mathbf{P}_{T2}^2\right)}\Bigg)\Bigg],\\
F_{kp3}^{\hat{M}\cdot D} &= C\left[\hat{M}\cdot D\,\frac{\left(\mathbf{P}_{T1}\cdot\mathbf{k}\right)\left(\mathbf{P}_{T2}\cdot p\right)-\left(\mathbf{P}_{T1}\cdot\mathbf{p}\right)\left(\mathbf{P}_{T2}\cdot\mathbf{k}\right)}{2\left(\mathbf{P}_{T1}^2\mathbf{P}_{T2}^2-\left(\mathbf{P}_{T1}\cdot\mathbf{P}_{T2}\right)^2\right)}\right],\\
F_{kp4}^{\hat{M}\cdot D} &= C\left[\hat{M}\cdot D\,\frac{\left(\mathbf{k}\cdot\mathbf{p}\right)\left(\left(\mathbf{P}_{T1}\cdot\mathbf{P}_{T2}\right)^2+\mathbf{P}_{T1}^2\mathbf{P}_{T2}^2\right)-\left(\mathbf{P}_{T2}\cdot\mathbf{k}\right)\left(\mathbf{P}_{T2}\cdot\mathbf{p}\right)\mathbf{P}_{T1}^2-\left(\mathbf{P}_{T1}\cdot\mathbf{k}\right)\left(\mathbf{P}_{T1}\cdot\mathbf{p}\right)\mathbf{P}_{T2}^2}{2\left(\mathbf{P}_{T1}\cdot\mathbf{P}_{T2}\right)^2}\right]
\end{aligned}\tag{87}$$

C. Simulation

The CLAS12 FAST-MC program was used to simulate the physics events and study the extraction of azimuthal moments and acceptance corrections. Events were generated with the clas12DIS generator [127], which is basically an implementation of the LUND Monte Carlo package called PEPSI (Polarized Electron-Proton Scattering Interactions) [128]. It is based on polarized and unpolarized parton distribution functions and the LUND string model for hadronization (both in target and current fragmentation region), and has been tested successfully against several low-Q^2 experiments with 5.7 GeV beam at Jefferson Lab.

A fast Monte Carlo simulation program has been used to define the acceptance and resolution of the CLAS12 detector with all of the standard (base) equipment in place. The kaons were assumed identified 100% in sectors covered by CLAS12-RICH, and also at energies above 5 GeV, where the pions start to fire

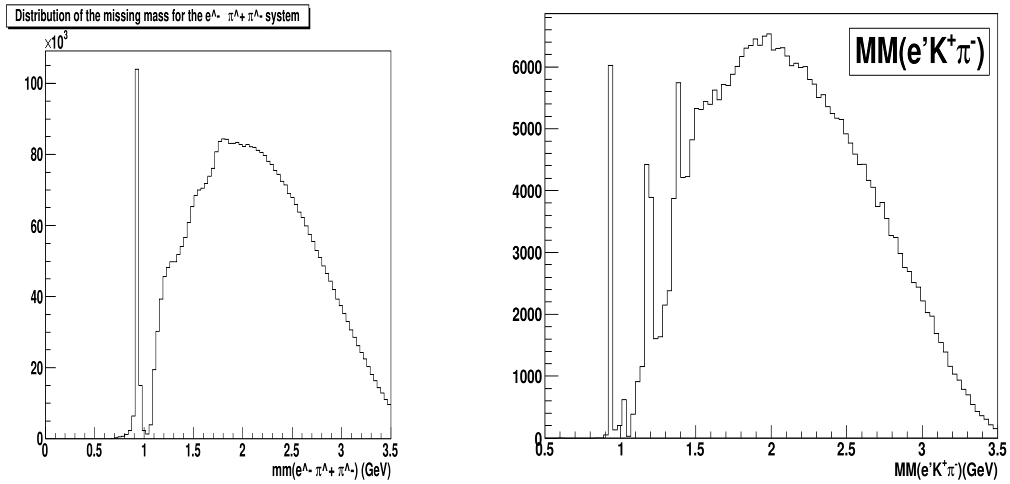

FIG. 26. Missing mass distributions for kaons and pion pairs from PEPSI MC for *ehhX* events.

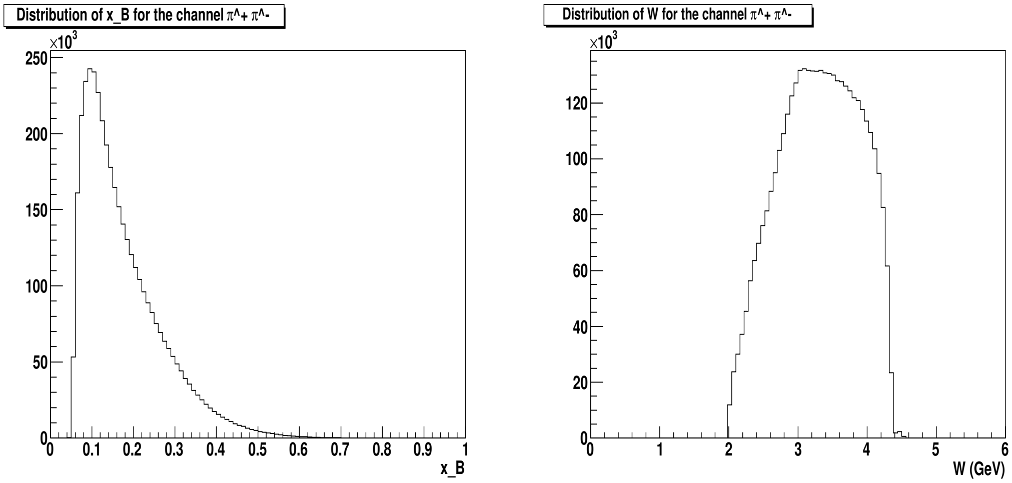

FIG. 27. x and W-distribution of pion pairs.

the High Threshold Cherekov Counter (HTCC). The events generated by clas12DIS are used as input and all particles are followed through all detector elements.

The resolution of the detector is simulated by a simple smearing function which modifies a particle's track by a random amount in momentum and angles according to a Gaussian distribution of the appropriate width. The amount of smearing follows the design specifications of the CLAS12 detector. The resolution in x varies between $0.01 < \sigma_x < 0.035$ and is therefore finer than our planned x bin size of 0.05 in all cases. Figures 26–33 show various kinematic distributions from this simulation.

A full Monte Carlo simulation (GEANT-based) of CLAS12 with all resolution effects will be used to determine the effective mean x (and Q^2) for each x-bin we will use to bin our data so we can accurately extract the x-dependence of the measured asymmetries.

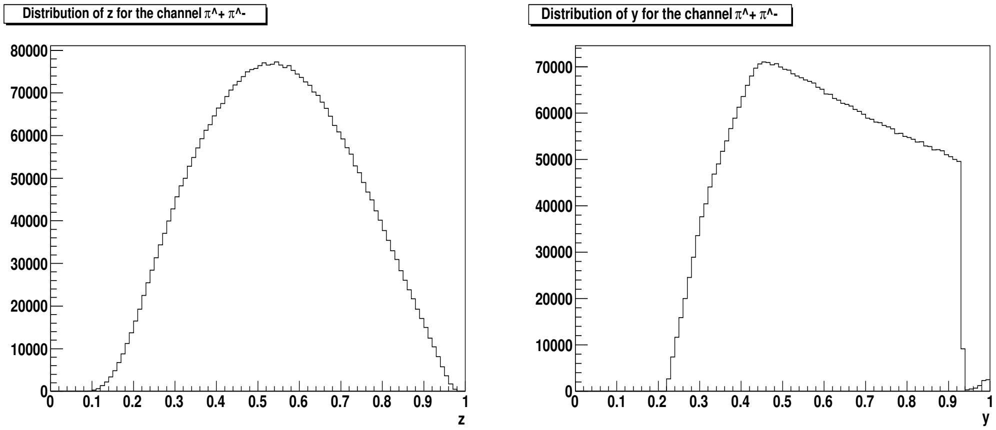

FIG. 28. z and y-distributions of pion pairs.

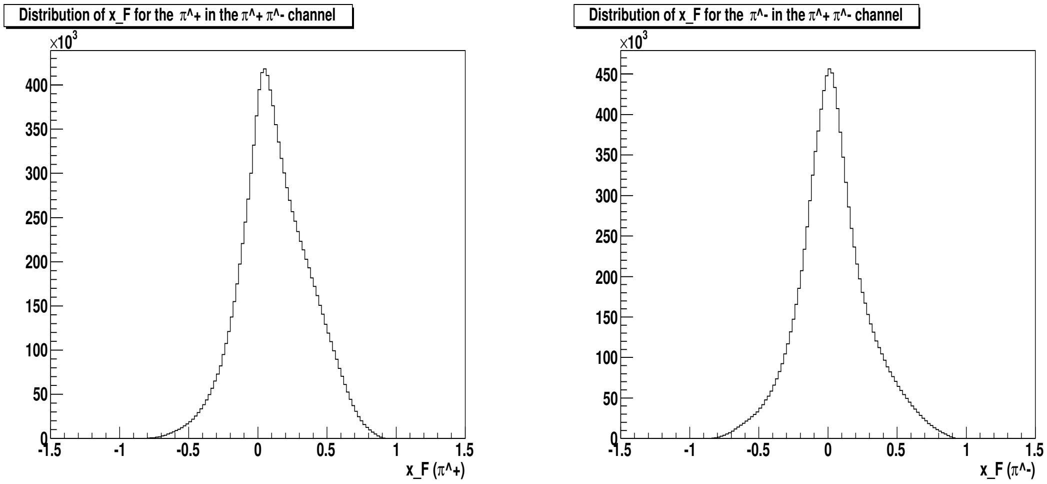

FIG. 29. x_F-distributions of π^+ (left) and π^- (right) of pion pairs.

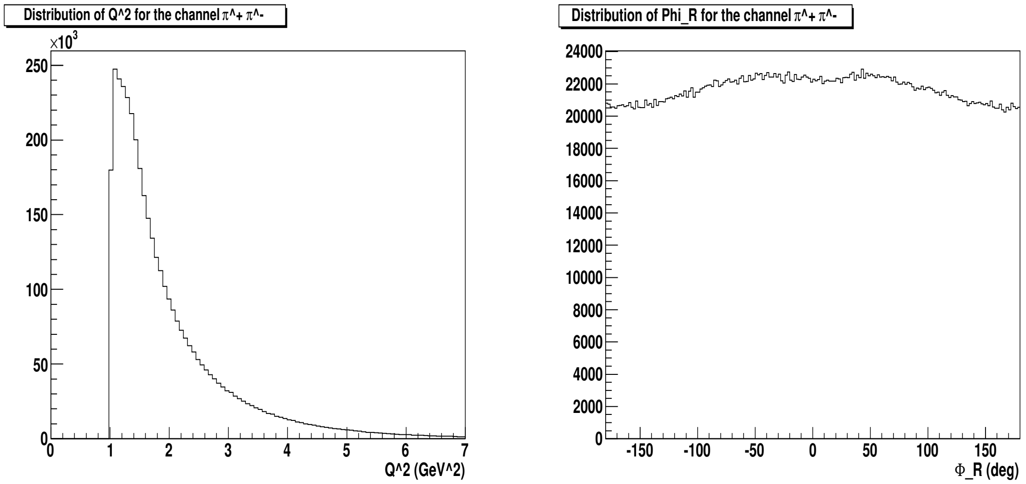

FIG. 30. The Q^2-distribution of pion pairs (left) and the ϕ_R-distribution of the pair (right).

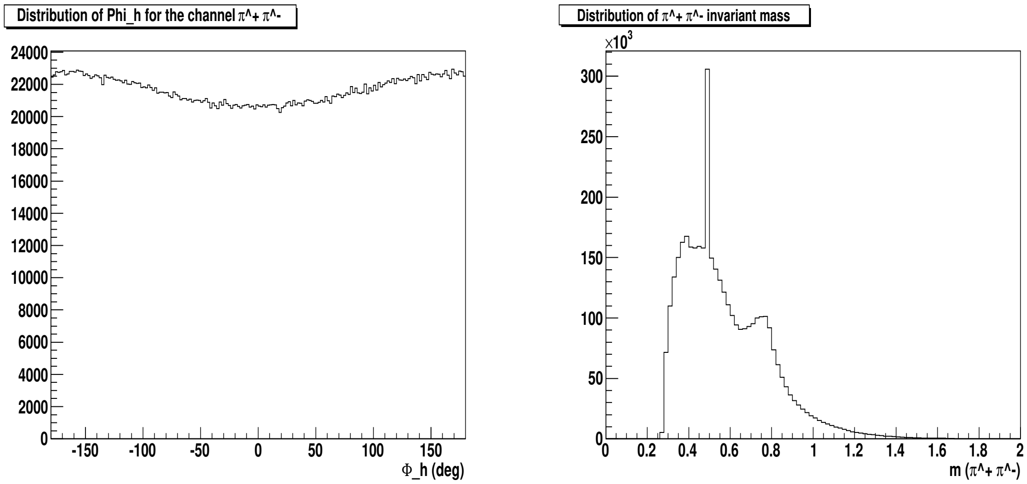

FIG. 31. The $\phi_h$distribution (left) and invariant mass distributions of the pair (right).

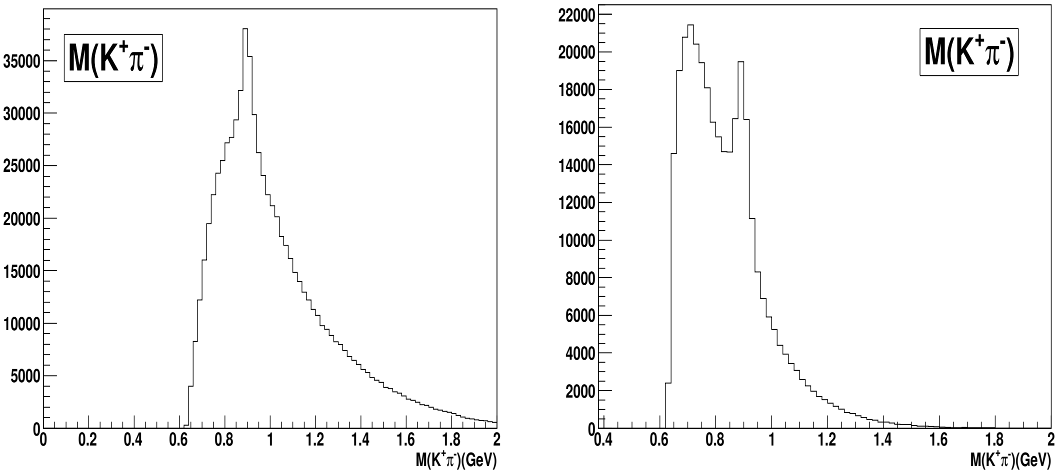

FIG. 32. Invariant masses for Kaon-pion pairs for tfr-cfr and cfr-cfr combinations

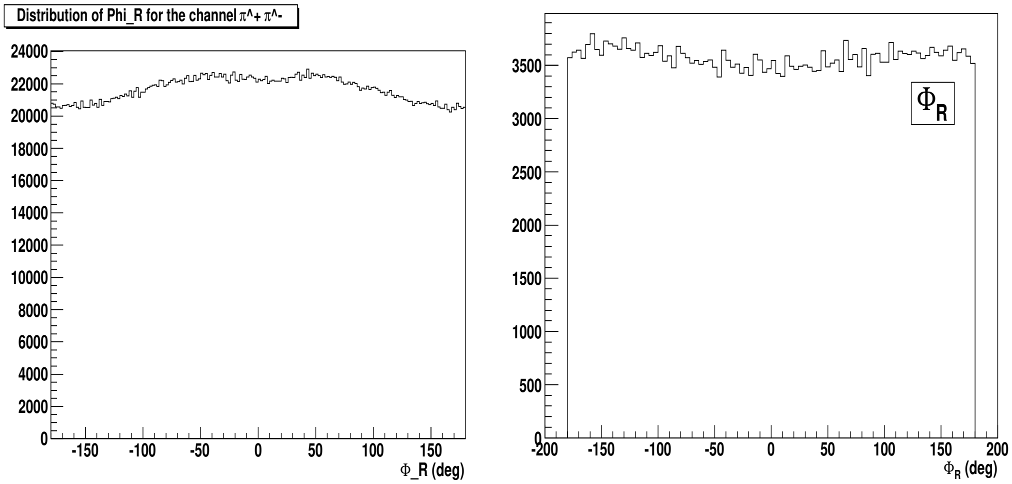

FIG. 33. Distribution over ϕ_R for pion-pion and pion-kaon pairs from FASTMC

---

[1] C. A. Aidala, S. D. Bass, D. Hasch, and G. K. Mallot, Rev. Mod. Phys. **85**, 655 (2013).
[2] A. Metz and A. Vossen, Prog. Part. Nucl. Phys. **91**, 136 (2016).
[3] S. A. Pereira (CLAS), *Proceedings, 22nd International Workshop on Deep-Inelastic Scattering and Related Subjects (DIS 2014): Warsaw, Poland, April 28-May 2, 2014*, PoS **DIS2014**, 231 (2014).
[4] S. Sirtl, in *22nd International Symposium on Spin Physics (SPIN 2016) Urbana, IL, USA, September 25-30, 2016* (2017) arXiv:1702.07317 [hep-ex].
[5] M. Boglione, J. Collins, L. Gamberg, J. O. Gonzalez-Hernandez, T. C. Rogers, and N. Sato, Phys. Lett. **B766**, 245 (2017), arXiv:1611.10329 [hep-ph].
[6] H. Avakian *et al.* (Jefferson Lab Hall B), PAC38 Proposal PR12-11-109 (2011).
[7] S. Kuhn *et al.*, JLab Experiment E12-06-109 (2006).
[8] H. Avakian *et al.*, JLab Experiment E12-07-107 (2007).
[9] K. Hafidi *et al.*, JLab Experiment E12-09-007 (2009).
[10] H. Avakian *et al.*, JLab Experiment E12-09-009 (2009).
[11] K. Kanazawa, Y. Koike, A. Metz, D. Pitonyak, and M. Schlegel, Phys. Rev. D **93**, 054024 (2016), arXiv:1512.07233 [hep-ph].
[12] R. L. Jaffe, Comments Nucl. Part. Phys. **19**, 239 (1990).
[13] M. Burkardt, Phys. Rev. D **88**, 114502 (2013), arXiv:0810.3589 [hep-ph].
[14] M. Abdallah and M. Burkardt, Phys. Rev. D **94**, 094040 (2016), arXiv:1610.01166 [hep-ph].
[15] A. Airapetian *et al.* (HERMES), Phys. Rev. Lett. **84**, 4047 (2000), hep-ex/9910062.
[16] A. Airapetian *et al.* (HERMES), Phys. Rev. **D64**, 097101 (2001), hep-ex/0104005.
[17] A. Airapetian *et al.* (HERMES), Phys. Lett. **B622**, 14 (2005), arXiv:hep-ex/0505042.
[18] H. Avakian *et al.* (The CLAS), Phys. Rev. Lett. **105**, 262002 (2010), arXiv:hep-ex/1003.4549 [hep-ex].
[19] M. G. Alekseev *et al.*, Eur. Phys. J. **C70**, 39 (2010), arXiv:1007.1562 [hep-ex].
[20] A. V. Efremov and P. Schweitzer, JHEP **08**, 006 (2003), arXiv:hep-ph/0212044.
[21] M. Anselmino and F. Murgia, Phys. Lett. **B483**, 74 (2000), arXiv:hep-ph/0002120.
[22] E. De Sanctis, W. D. Nowak, and K. A. Oganesian, Phys. Lett. **B483**, 69 (2000), arXiv:hep-ph/0002091.
[23] A. V. Efremov, K. Goeke, M. V. Polyakov, and D. Urbano, Phys. Lett. **B478**, 94 (2000), arXiv:hep-ph/0001119.
[24] K. A. Oganessian, N. Bianchi, E. De Sanctis, and W. D. Nowak, Nucl. Phys. **A689**, 784 (2001), arXiv:hep-ph/0010261.
[25] A. V. Efremov, K. Goeke, and P. Schweitzer, Phys. Lett. **B522**, 37 (2001), arXiv:hep-ph/0108213.
[26] A. V. Efremov, K. Goeke, and P. Schweitzer, Eur. Phys. J. **C24**, 407 (2002), arXiv:hep-ph/0112166.
[27] A. V. Efremov, K. Goeke, and P. Schweitzer, Eur. Phys. J. **C32**, 337 (2003), arXiv:hep-ph/0309209.
[28] P. Schweitzer and A. Bacchetta, Nucl. Phys. **A732**, 106 (2004), arXiv:hep-ph/0310318.
[29] A. V. Efremov, K. Goeke, and P. Schweitzer, Phys. Lett. **B568**, 63 (2003), arXiv:hep-ph/0303062.
[30] B.-Q. Ma, I. Schmidt, and J.-J. Yang, Phys. Rev. **D65**, 034010 (2002), arXiv:hep-ph/0110324.
[31] A. V. Efremov, K. Goeke, and P. Schweitzer, Phys. Rev. **D67**, 114014 (2003), hep-ph/0208124.
[32] U. D'Alesio and F. Murgia, Phys.Rev. **D70**, 074009 (2004), arXiv:hep-ph/0408092 [hep-ph].
[33] F. Yuan, Phys. Lett. **B589**, 28 (2004), hep-ph/0310279.
[34] A. Afanasev and C. Carlson, in *8th Conference on the Intersections of Particle and Nuclear Physics* (2003) arXiv:hep-ph/0308163.
[35] A. Bacchetta, P. J. Mulders, and F. Pijlman, Phys. Lett. **B595**, 309 (2004), arXiv:hep-ph/0405154.
[36] L. P. Gamberg, D. S. Hwang, A. Metz, and M. Schlegel, Phys. Lett. **B639**, 508 (2006), arXiv:hep-ph/0604022.
[37] A. Bacchetta, D. Boer, M. Diehl, and P. J. Mulders, JHEP **08**, 023 (2008), arXiv:hep-ph/0803.0227 [hep-ph].
[38] R. L. Jaffe, X.-m. Jin, and J. Tang, Phys. Rev. Lett. **80**, 1166 (1998), arXiv:hep-ph/9709322.
[39] A. Bianconi, S. Boffi, R. Jakob, and M. Radici, Phys. Rev. **D62**, 034008 (2000), arXiv:hep-ph/9907475.
[40] M. Radici, R. Jakob, and A. Bianconi, Phys. Rev. **D65**, 074031 (2002), arXiv:hep-ph/0110252.
[41] A. Bacchetta and M. Radici, Phys. Rev. **D67**, 094002 (2003), arXiv:hep-ph/0212300.
[42] A. Bacchetta and M. Radici, Phys. Rev. **D69**, 074026 (2004), arXiv:hep-ph/0311173.
[43] A. Bacchetta and M. Radici, Phys. Rev. **D74**, 114007 (2006), arXiv:hep-ph/0608037.
[44] F. A. Ceccopieri, M. Radici, and A. Bacchetta, Phys. Lett. **B650**, 81 (2007), arXiv:hep-ph/0703265.
[45] A. Bacchetta, A. Courtoy, and M. Radici, Phys. Rev. Lett. **107**, 012001 (2011), arXiv:1104.3855 [hep-ph].
[46] L. Trentadue and G. Veneziano, Phys. Lett. **B323**, 201 (1994).
[47] M. Anselmino, V. Barone, and A. Kotzinian, Phys. Lett. **B699**, 108 (2011), arXiv:1102.4214 [hep-ph].
[48] S. Gliske, A. Bacchetta, and M. Radici, Phys. Rev. **D90**, 114027 (2014), [Erratum: Phys. Rev.D91,no.1,019902(2015)], arXiv:1408.5721 [hep-ph].
[49] A. Bacchetta *et al.*, JHEP **02**, 093 (2007), arXiv:hep-ph/0611265.
[50] A. Bacchetta, U. D'Alesio, M. Diehl, and C. A. Miller, Phys. Rev. **D70**, 117504 (2004), arXiv:hep-ph/0410050.
[51] M. Diehl and S. Sapeta, Eur. Phys. J. **C41**, 515 (2005), arXiv:hep-ph/0503023.
[52] J. Zhou and A. Metz, Phys. Rev. Lett. **106**, 172001 (2011), arXiv:1101.3273 [hep-ph].

[53] S. Wandzura and F. Wilczek, Phys. Lett. **B72**, 195 (1977).
[54] R. Tangerman and P. Mulders, (1994), arXiv:hep-ph/9408305.
[55] P. J. Mulders and R. D. Tangerman, Nucl. Phys. **B461**, 197 (1996), hep-ph/9510301.
[56] H. Avakian *et al.*, Phys. Rev. **D77**, 014023 (2008), arXiv:hep-ph/0709.3253 [hep-ph].
[57] A. Metz, P. Schweitzer, and T. Teckentrup, Phys. Lett. B **680**, 141 (2009), arXiv:0810.5212 [hep-ph].
[58] R. L. Jaffe and X.-D. Ji, Phys. Rev. **D43**, 724 (1991).
[59] A. Harindranath and W.-M. Zhang, Phys. Lett. **B408**, 347 (1997), arXiv:hep-ph/9706419.
[60] R. Kundu and A. Metz, Phys. Rev. **D65**, 014009 (2002), arXiv:hep-ph/0107073.
[61] A. Accardi, A. Bacchetta, W. Melnitchouk, and M. Schlegel, JHEP **11**, 093 (2009), arXiv:0907.2942 [hep-ph].
[62] A. Vossen *et al.* (BELLE Collaboration), Phys.Rev.Lett. (2011), arXiv:1104.2425 [hep-ex].
[63] W. Yang, X. Wang, Y. Yang, and Z. Lu, Phys. Rev. **D99**, 054003 (2019), arXiv:1902.07889 [hep-ph].
[64] A. Courtoy, (2014), arXiv:1405.7659 [hep-ph].
[65] S. Pisano and M. Radici, Eur. Phys. J. **A52**, 155 (2016), arXiv:1511.03220 [hep-ph].
[66] A. Airapetian *et al.* (HERMES), JHEP **06**, 017 (2008), arXiv:0803.2367 [hep-ex].
[67] A. Bianconi, S. Boffi, R. Jakob, and M. Radici, Phys. Rev. **D62**, 034009 (2000), arXiv:hep-ph/9907488.
[68] A. Bacchetta, F. A. Ceccopieri, A. Mukherjee, and M. Radici, Phys. Rev. **D79**, 034029 (2009), arXiv:0812.0611 [hep-ph].
[69] X. Artru and J. C. Collins, Z. Phys. **C69**, 277 (1996), arXiv:hep-ph/9504220.
[70] A. Courtoy, A. Bacchetta, M. Radici, and A. Bianconi, Phys. Rev. D **85**, 114023 (2012), arXiv:1202.0323 [hep-ph].
[71] R. L. Jaffe and X.-D. Ji, Nucl. Phys. **B375**, 527 (1992).
[72] A. I. Signal, Nucl. Phys. **B497**, 415 (1997), arXiv:hep-ph/9610480.
[73] H. Avakian, A. V. Efremov, P. Schweitzer, and F. Yuan, Phys. Rev. **D81**, 074035 (2010), arXiv:hep-ph/1001.5467 [hep-ph].
[74] R. Jakob, P. J. Mulders, and J. Rodrigues, Nucl. Phys. **A626**, 937 (1997), hep-ph/9704335.
[75] J. Balla, M. V. Polyakov, and C. Weiss, Nucl. Phys. **B510**, 327 (1998), arXiv:hep-ph/9707515.
[76] B. Dressler and M. V. Polyakov, Phys. Rev. **D61**, 097501 (2000), arXiv:hep-ph/9912376.
[77] M. Wakamatsu, Phys. Lett. **B509**, 59 (2001), arXiv:hep-ph/0012331.
[78] P. Schweitzer, Phys. Rev. **D67**, 114010 (2003), arXiv:hep-ph/0303011.
[79] M. Wakamatsu and Y. Ohnishi, Phys. Rev. **D67**, 114011 (2003), arXiv:hep-ph/0303007.
[80] Y. Ohnishi and M. Wakamatsu, Phys. Rev. **D69**, 114002 (2004), arXiv:hep-ph/0312044.
[81] C. Cebulla, J. Ossmann, P. Schweitzer, and D. Urbano, Acta Phys. Polon. **B39**, 609 (2008), arXiv:0710.3103 [hep-ph].
[82] M. Burkardt and Y. Koike, Nucl. Phys. **B632**, 311 (2002), arXiv:hep-ph/0111343.
[83] A. Mukherjee, Phys. Lett. **B687**, 180 (2010), arXiv:0912.1446 [hep-ph].
[84] P. Schweitzer *et al.*, Phys. Rev. **D64**, 034013 (2001), arXiv:hep-ph/0101300.
[85] D. Boer, R. Jakob, and M. Radici, Phys. Rev. **D67**, 094003 (2003), arXiv:hep-ph/0302232.
[86] H. H. Matevosyan, A. Kotzinian, and A. W. Thomas, Phys. Rev. **D96**, 074010 (2017), arXiv:1707.04999 [hep-ph].
[87] H. H. Matevosyan, A. Kotzinian, and A. W. Thomas, Phys. Rev. **D97**, 014019 (2018), arXiv:1709.08643 [hep-ph].
[88] X. Luo, H. Sun, and Y.-L. Xie, Phys. Rev. **D101**, 054020 (2020), arXiv:2003.03770 [hep-ph].
[89] A. Abdesselam *et al.* (Belle), (2015), arXiv:1505.08020 [hep-ex].
[90] H. H. Matevosyan, A. Bacchetta, D. Boer, A. Courtoy, A. Kotzinian, M. Radici, and A. W. Thomas, Phys. Rev. D **97**, 074019 (2018), arXiv:1802.01578 [hep-ph].
[91] H. Matevosyan, PoS **DIS2018**, 150 (2018), arXiv:1807.11485 [hep-ph].
[92] H. H. Matevosyan, A. Kotzinian, and A. W. Thomas, Phys. Rev. Lett. **120**, 252001 (2018), arXiv:1712.06384 [hep-ph].
[93] A. Kotzinian, M. Anselmino, and V. Barone, Nuovo Cim. C **036**, 127 (2013), arXiv:1303.2461 [hep-ph].
[94] A. Kotzinian, M. Anselmino, and V. Barone, in *19th International Workshop on Deep-Inelastic Scattering and Related Subjects* (2011) arXiv:1107.2292 [hep-ph].
[95] H. Avakian and S. Pisano, PoS **DIS2016**, 214 (2016).
[96] V. Burkert *et al.*, Nucl. Instrum. Meth. A **959**, 163419 (2020).
[97] V. Ziegler *et al.*, Nucl. Instrum. Meth. A **959**, 163472 (2020).
[98] Y. Sharabian *et al.*, Nucl. Instrum. Meth. A **968**, 163824 (2020).
[99] M. Ungaro *et al.*, Nucl. Instrum. Meth. A **957**, 163420 (2020).
[100] D. Carman *et al.*, Nucl. Instrum. Meth. A **960**, 163629 (2020).
[101] D. Carman, G. Asryan, V. Baturin, L. Clark, R. De Vita, W. Kim, B. Miller, and C. Wiggins, Nucl. Instrum. Meth. A **960**, 163626 (2020).
[102] M. Contalbrigo *et al.*, Nucl. Instrum. Meth. A **964**, 163791 (2020).
[103] J. Brock, PoS **SPIN2018**, 101 (2018).

[104] C. Keith, PoS **PSTP2017**, 008 (2017).
[105] C. D. Keith *et al.*, Nucl. Instrum. Meth. **A501**, 327 (2003).
[106] R. Milner *et al.*, PAC48 Proposal (2020).
[107] J. Maxwell and R. Milner, (2019), arXiv:1911.06650 [physics.ins-det].
[108] J. Maxwell, PoS **SPIN2018**, 102 (2018).
[109] R. N. Cahn, Phys. Lett. **B78**, 269 (1978).
[110] E. L. Berger, Z. Phys. **C4**, 289 (1980).
[111] A. Brandenburg, V. V. Khoze, and D. Mueller, Phys. Lett. **B347**, 413 (1995), arXiv:hep-ph/9410327.
[112] A. Afanasev, C. E. Carlson, and C. Wahlquist, Phys. Lett. **B398**, 393 (1997), hep-ph/9701215.
[113] S. J. Brodsky, M. Diehl, P. Hoyer, and S. Peigne, Phys. Lett. **B449**, 306 (1999), arXiv:hep-ph/9812277.
[114] I. Akushevich, N. Shumeiko, and A. Soroko, Eur. Phys. J. **C10**, 681 (1999), arXiv:hep-ph/9903325.
[115] I. Akushevich, A. Ilyichev, and M. Osipenko, Phys. Lett. B **672**, 35 (2009), arXiv:0711.4789 [hep-ph].
[116] B. Raydo, S. Boyarinov, A. Celentano, C. Cuevas, R. de Vita, V. Kubarovsky, B. Moffit, S. Niccolai, R. Paremuzyan, and C. Smith, Nucl. Instrum. Meth. A **960**, 163529 (2020).
[117] K. V. Dharmawardane *et al.* (CLAS), Phys. Lett. **B641**, 11 (2006), nucl-ex/0605028.
[118] M. Mirazita, H. Avakian, A. Courtoy, and S. Pisano (CLAS), (2020), in preparation.
[119] R. J. Barlow, Nucl. Instrum. Meth. A **297**, 496 (1990).
[120] A. Bacchetta, A. Courtoy, and M. Radici, JHEP **03**, 119 (2013), arXiv:1212.3568 [hep-ph].
[121] M. Radici, A. Courtoy, A. Bacchetta, and M. Guagnelli, JHEP **05**, 123 (2015), arXiv:1503.03495 [hep-ph].
[122] J. Benel, A. Courtoy, and R. Ferro-Hernandez, Eur. Phys. J. C **80**, 465 (2020), arXiv:1912.03289 [hep-ph].
[123] C. Dilks (Presented at APS DNP2019, 2019).
[124] T. Hayward (Presented at APS DNP2019, 2019).
[125] G. Gilfoil *et al.*, JLab Experiment E12-07-104 (2007).
[126] M. Arneodo *et al.* (European Muon), Z. Phys. **C34**, 277 (1987).
[127] H. Avakian and P. Bosted., (2006).
[128] L. Mankiewicz, A. Schafer, and M. Veltri, Comput. Phys. Commun. **71**, 305 (1992).